Article

In Situ Time-Resolved FRET Reveals Effects of Sarcomere Length on Cardiac Thin-Filament Activation

King-Lun Li,[1] Daniel Rieck,[1] R. John Solaro,[3] and Wenji Dong[1,2,*]

[1]Gene and Linda Voiland School of Chemical Engineering and Bioengineering and [2]Integrative Neuroscience and Physiology, Washington State University, Pullman, Washington; and [3]The Department of Physiology and Biophysics, Center for Cardiovascular Research, College of Medicine, University of Illinois at Chicago, Chicago, Illinois

ABSTRACT During cardiac thin-filament activation, the N-domain of cardiac troponin C (N-cTnC) binds to Ca^{2+} and interacts with the actomyosin inhibitory troponin I (cTnI). The interaction between N-cTnC and cTnI stabilizes the Ca^{2+}-induced opening of N-cTnC and is presumed to also destabilize cTnI–actin interactions that work together with steric effects of tropomyosin to inhibit force generation. Recently, our in situ steady-state FRET measurements based on N-cTnC opening suggested that at long sarcomere length, strongly bound cross-bridges indirectly stabilize this Ca^{2+}-sensitizing N-cTnC–cTnI interaction through structural effects on tropomyosin and cTnI. However, the method previously used was unable to determine whether N-cTnC opening depends on sarcomere length. In this study, we used time-resolved FRET to monitor the effects of cross-bridge state and sarcomere length on the Ca^{2+}-dependent conformational behavior of N-cTnC in skinned cardiac muscle fibers. FRET donor (AEDANS) and acceptor (DDPM)-labeled double-cysteine mutant cTnC(T13C/N51C)$_{AEDANS\text{-}DDPM}$ was incorporated into skinned muscle fibers to monitor N-cTnC opening. To study the structural effects of sarcomere length on N-cTnC, we monitored N-cTnC opening at relaxing and saturating levels of Ca^{2+} and 1.80 and 2.2-μm sarcomere length. Mg^{2+}-ADP and orthovanadate were used to examine the structural effects of noncycling strong-binding and weak-binding cross-bridges, respectively. We found that the stabilizing effect of strongly bound cross-bridges on N-cTnC opening (which we interpret as transmitted through related changes in cTnI and tropomyosin) become diminished by decreases in sarcomere length. Additionally, orthovanadate blunted the effect of sarcomere length on N-cTnC conformational behavior such that weak-binding cross-bridges had no effect on N-cTnC opening at any tested [Ca^{2+}] or sarcomere length. Based on our findings, we conclude that the observed sarcomere length-dependent positive feedback regulation is a key determinant in the length-dependent Ca^{2+} sensitivity of myofilament activation and consequently the mechanism underlying the Frank-Starling law of the heart.

INTRODUCTION

Regulation of cardiac muscle contraction requires the Ca^{2+}-dependent, integrated activity of highly synchronized and fine-tuned thin-filament protein-protein interactions, many of which involve the cardiac troponin (cTn) complex. To activate the thin filament at the beginning of systole, Ca^{2+} binds to the N-domain of cTnC (N-cTnC). This initiates a series of intra- and intermolecular structural changes in thin-filament proteins (1–3), including partially exposing a previously buried hydrophobic patch in N-cTnC (4–6), followed by the interaction between the hydrophobic patch and the switch region of cTnI (cTnI-Sr). This interaction switches the actomyosin-inhibitory C-terminal domain of cTnI away from interacting with actin toward interacting with N-cTnC (4,5,7–12) and further stabilizes Ca^{2+}-induced N-cTnC opening (4,5,11,13). The detachment of cTnI from actin leads to tropomyosin shifting from the blocked toward the closed state of thin-filament regulation, a transition in which cTnT also plays a role (14). Ultimately, it is this shifting of tropomyosin toward the closed state that enables the strong attachment of cross-bridges to actin to generate force (15–20). (See Table 1 for Glossary of General Terms used in this article.)

Interestingly, such force-generating strong actomyosin interactions induce further structural changes in the thin filament that sensitize it to Ca^{2+} in what is termed "positive feedback regulation" (21–24). This feedback activation pathway is thought to arise from the ability of strong myosin head binding to actin to shift tropomyosin toward the open state (25), which concomitantly disrupts cTnI–actin interactions even in the absence of Ca^{2+} (11,12). These structural changes indirectly stabilize N-cTnC opening through strengthening the N-cTnC–cTnI-Sr interaction (13,26), which is known to be important for stabilizing N-cTnC in the open conformation, as mentioned above (4,5).

Recently, a fourth state of thin-filament regulation has even been proposed to account for such Ca^{2+} independent activation of thin-filament regulatory units by myosin heads (27). In the fourth state, tropomyosin is in the open state of thin-filament regulation and cTnI-Sr can thus interact with N-cTnC, but Ca^{2+} is not bound to cTnC site II. To more fully understand the molecular mechanisms underlying these processes, our group has previously used in vitro

Submitted December 16, 2013, and accepted for publication May 13, 2014.

*Correspondence: wdong@vetmed.wsu.edu

Editor: Bernhard Brenner.

0006-3495/14/08/0682/12 $2.00

http://dx.doi.org/10.1016/j.bpj.2014.05.044

TABLE 1 Glossary of general abbreviations

Term	Definition
BDM	2, 3-butanedione monoxime
c	Cardiac muscle
DDPM	*N*-(4-dimethylamino-3,5-dinitrophenyl)maleimide
DTT	Dithiothreitol
EDTA	Ethylenediaminetetraacetic acid
EGTA	Ethylene glycol-bis-(β-aminoethyl ether)-*N*,*N*,*N*′,*N*′-tetraacetic acid
FRET	Förster resonance energy transfer
AEDANS	5-(io-doacetamidoethyl)aminonaphthelene-1-sulfonic acid
Tn	Troponin
TnC	Troponin C
TnI	Troponin I
TnT	Troponin T
S1	Myosin subfragment-1

fluorescence spectroscopy techniques to extensively study and characterize the distinct protein conformational changes that serve as the biophysical basis for thin-filament and positive feedback regulation (8–12,28–31). In these studies and in related work by others (20,32–36), a vast amount of information on how conformational changes in cTnC and cTnI participate in the molecular mechanism underlying cardiac thin-filament regulation has been uncovered using in vitro, reconstituted, thin filaments. An ongoing question is how well this information will hold in the context of the myofilament lattice found in myocardial sarcomeres (hereafter referred to as "in situ").

While important information has been uncovered using reconstituted thin filaments, they lack important features of the myofilament lattice, including a loaded condition and lattice-associated geometric and mechanical constraints on protein structure and function. To study thin-filament regulation under a more-nearly native setting, we recently implemented steady-state Förster resonance energy transfer (ss-FRET) in detergent-skinned cardiac muscle fibers and used it to monitor in situ N-cTnC opening (37). Our results demonstrated that strong cross-bridge binding to actin leads to a stabilization of N-cTnC opening. Because stabilizing the open conformation of N-cTnC increases Ca^{2+} sensitivity (38–42), this finding provides a structural explanation for the thin-filament Ca^{2+}-sensitizing effect of positive feedback regulation. Due to the fluorophore-concentration-dependent nature of our in situ ss-FRET technique, we did not further investigate an additional important mechanism to positive feedback regulation—one that further modulates thin-filament activation in vivo—namely, cardiac myofilament length-dependent activation (43–45).

Length-dependent activation is thought to underlie the Frank-Starling law of the heart, which describes the increase in stroke volume that occurs in response to an increase in diastolic ventricular filling (46). Increased filling stretches the myocardium, producing an increase in sarcomere length (SL) that leads to myofilament-length-dependent activation wherein the maximum tension developed by myofilaments is increased and their response to Ca^{2+} is enhanced. Accordingly, in this study we investigate the effect of changes in SL on cardiac thin-filament activation at the molecular level. Recent studies have shown that the maximum extent of ensemble-averaged N-cTnC opening within thin-filament regulatory units is positively correlated with thin-filament Ca^{2+} sensitivity (37,47), and as discussed above, strong actomyosin interactions lead to a stabilization of N-cTnC opening.

Additionally, recent small-angle x-ray diffraction evidence reported by Farman et al. (48) has suggested that increased SL leads to structural changes in thick-filament myosin heads that should promote increased interaction between strong-binding cross-bridges and actin. Thus, we hypothesized that a decrease in SL should produce decreased interaction between strong-binding cross-bridges and actin, which should consequently lead to decreased force and ensemble-averaged N-cTnC opening. Furthermore, we reasoned that changes in SL should produce no effect on N-cTnC opening when strong-binding cross-bridges are absent.

Although fluorescence intensity of a fluorophore is concentration-dependent, its fluorescence lifetime is not. Thus, to test our hypothesis that a decrease in SL would decrease N-cTnC opening, we have developed an in situ time-resolved FRET (tr-FRET) technique by retrofitting our Güth muscle research system (MRS) with time-correlated single-photon counting technology. This modification of the MRS allows us to perform fluorescence lifetime measurements of AEDANS-labeled cTnC incorporated into fiber samples to determine the effects of SL changes on in situ N-TnC opening. Accordingly, isometric tr-FRET experiments were performed on skinned fibers wherein endogenous cTnC was replaced with the double cysteine cTnC(T13C/N51C) mutant labeled with AEDANS and DDPM as FRET donor and acceptor, respectively. The roles that strong- and weak-binding cross-bridges play in Ca^{2+}- and length-dependent activation were tested by promoting or inhibiting strong cross-bridge binding with Mg^{2+}-ADP and sodium orthovanadate (Vi), respectively.

Fluorescence intensity decays yielded from these tr-FRET experiments were used to determine AEDANS-DDPM distance distributions as a function of cTnC site-II Ca^{2+} occupancy, cross-bridge states, and SL. AEDANS-DDPM-modified cTnC indicated that the ensemble-averaged extent of N-cTnC opening was not only dependent on Ca^{2+} occupancy and cross-bridge state, but also on SL. Specifically, reduction of SL attenuated the stabilizing effects of strong-binding cross-bridges on N-cTnC opening, and treatment with Vi eliminated SL-dependent changes in N-cTnC opening altogether. Thus, modulation of positive feedback regulation by SL was shown to be mechanistically involved in the length-dependent Ca^{2+} sensitivity associated with myofilament length-dependent activation.

MATERIALS AND METHODS

Animal handling protocols

The handling of all the experimental animals followed the institutional guidelines and protocols approved by the Animal Care and Use Committee and the Office of Laboratory Animal Welfare, National Institutes of Health, Bethesda, MD. Our muscle-fiber study also followed the established guidelines of, and was approved by, the Washington State University Institutional Animal Care and Use Committee.

Experimental preparations

Methods based on previously reported protocols (37) were followed for tissue dissection; preparation of proteins, highly relaxing solution, pCa 9 and 4.3 solutions, and pCa solutions containing either Vi or ADP, and detergent-skinned fibers; cTnC extraction and reconstitution; and characterization of reconstitution efficiency using sodium dodecyl sulfate polyacrylamide gel electrophoresis and Western blotting. See the Supporting Material for further details.

Simultaneous measurement of isometric force and time-resolved fluorescence intensity in detergent-skinned cardiac muscle fibers

The same measurement protocol as described in our Supporting Material was used to perform simultaneous measurements of force and tr-FRET of N-cTnC opening as a function of cTnC site-II Ca^{2+} occupancy, SL, and cross-bridge state. Tested cross-bridge states included cycling cross-bridges; Mg^{2+}-ADP-induced noncycling, strong-binding cross-bridges; or Vi-induced noncycling, weak-binding cross-bridges. There are some important experimental design considerations for using Vi to inhibit strong cross-bridge binding (see the Supporting Material for further details) (49–52), and we have previously demonstrated that the method works reliably under our experimental conditions (37). This was confirmed here by the fact that by following the tr-FRET measurement protocol and regardless of test condition, maximal force could be recovered on average to 88.0 ± 2.3%. Furthermore, no significant change in passive tension at pCa 9 was observed by following the tr-FRET measurement protocol conducted under any of the conditions tested.

Fig. S1 in the Supporting Material shows typical recordings of intensity decays (see Fig. S1 *A*) and isometric force traces (see Fig. S1 *B*) that were obtained using the protocol. As consistent with our prior ss-FRET observations (11,31,37), the fluorescence intensity decay of AEDANS observed in fibers containing donor-only-labeled cTnC(T13C/N51C)$_{AEDANS}$, was insensitive to changes in Ca^{2+} concentration and cross-bridge attachment (see Fig. S1 *A*, *inset*), whereas the intensity decay from fibers containing cTnC(T13C/N51C)$_{AEDANS\text{-}DDPM}$ showed significant changes that were indicative of N-cTnC opening in response to elevated Ca^{2+} concentrations and strong cross-bridge binding (see Fig. S1 *A*). For example, in cTnC(T13C/N51C)$_{AEDANS\text{-}DDPM}$-reconstituted fibers in the normal resting state (pCa 9.0), the AEDANS excited-state lifetime was appreciably reduced due to FRET with DDPM (see Fig. S1 *A*, *gray dots without lines* versus those *with lines*). Upon activation of the fibers with Ca^{2+} (pCa 4.3), the fluorescence lifetime was substantially recovered (see Fig. S1 *A*, *dashed lines* versus *solid lines*), which suggested that a Ca^{2+}-induced reduction in FRET had been caused by increased ensemble-averaged separation between AEDANS and DDPM.

Decay traces were used to calculate the distribution of interprobe distances between AEDANS and DDPM using the equations described in our Supporting Material. The global analysis procedure described therein yields a distribution of intersite distances to which an observed AEDANS excited-state decay is attributed. Measurements of the anisotropy of AEDANS under each test condition were used to ensure that the average orientations of the probes attached to Cys-13 and Cys-51 did not change significantly between different test conditions (see Fig. S2). Fig. 1 shows a typical distribution produced by decay fitting (*A*) with residue and autocorrelation analysis and distance distributions (*B*) recovered from observations made at 2.2 μm SL. The distance at the peak of the distribution was taken as the mean distance (r) between donor and acceptor sites within the N-cTnC population being observed. The spread of the distance distribution is described by a half-width at half-maximum (HWHM). Fitted values of r and HWHM were compared with the use of Student's t-test, with significance at the 95% confidence level ($p < 0.05$).

RESULTS

In situ time-resolved FRET measurements of the opening of the N-domain of cTnC and its analysis

To test our hypothesis that positive-feedback regulation is modulated by changes in SL, the in situ conformational behavior of N-cTnC was quantitatively characterized using tr-FRET measurements performed on cTnC(T13C/N51C)$_{AEDANS}$- and cTnC(T13C/N51C)$_{AEDANS\text{-}DDPM}$-reconstituted myocardial fibers. Densitometric analysis of Western blots using cTnC-specific antibodies (see Fig. S3) indicated that >85% of endogenous cTnC was replaced with fluorescently labeled cTnC constructs, which was similar to the reconstitution efficiency reported previously (37). Our tr-FRET experiments on these fibers were designed to evaluate the interrelationship between the effects of cTnC site-II Ca^{2+}-occupancy, cross-bridge binding state, and SL on the conformational behavior of N-cTnC. The AEDANS intensity decay observed under each test condition was analyzed in terms of a Cys-13–Cys-51 distance distribution from which r and HWHM were derived (see Materials and Methods). Fitted distribution parameters recovered from analysis of intensity decays are summarized in Table 2 (normalized values are also given in Table S1 in the Supporting Material), wherein the r was taken from where the peak of the distribution fell. As described below, changes in r and HWHM were used to evaluate the effects of changes in pCa, cross-bridge

TABLE 2 Cys-13–Cys-51 distance distributions observed in cTnC(N13C/T51C)$_{AEDANS\text{-}DDPM}$-reconstituted fibers under different biochemical conditions

Cross-bridge state	pCa	r[a] (Å)		HWHM[b] (Å)	
		1.8 μm SL	2.2 μm SL	1.8 μm SL	2.2 μm SL
5 mM ATP	9.0	26.21 ± 0.27	25.53 ± 0.29	6.23 ± 0.64	7.19 ± 0.07
	4.3	31.42 ± 0.42	32.97 ± 0.25	5.52 ± 0.42	8.05 ± 0.37
1 mM Vi[a]	9.0	25.46 ± 0.12	25.07 ± 0.10	5.11 ± 0.62	5.52 ± 0.20
	4.3	29.97 ± 0.40	29.83 ± 0.31	5.15 ± 0.31	5.85 ± 0.26
5 mM ADP[b]	9.0	25.70 ± 0.39	26.72 ± 0.16	5.74 ± 0.45	4.39 ± 0.19
	4.3	31.80 ± 0.14	33.78 ± 0.08	5.48 ± 0.56	3.78 ± 0.71
0.5 mM Vi[a]	9.0	—	25.75 ± 0.19	—	6.57 ± 0.12
	4.3	—	32.03 ± 0.18	—	5.43 ± 0.43
2.5 mM ADP[b]	9.0	—	26.39 ± 0.26	—	5.18 ± 0.10
	4.3	—	33.28 ± 0.22	—	6.41 ± 0.37

Absolute parameter values are given as mean ± SE.
[a]Vi solutions also contained 5 mM ATP.
[b]ATP was absent in ADP solutions.

binding state, or SL on the conformational behavior of N-cTnC.

Because of the locations of Cys-13 and Cys-51 within the quaternary structure of N-cTnC, *r* is interpreted to represent the ensemble-averaged extent of N-cTnC hydrophobic patch exposure (37). Therefore, *r* can increase when a greater proportion of the N-cTnC ensemble transitions from the closed conformation of N-cTnC (53) to the open conformation (4). HWHM represents the breadth of the range of Cys-13–Cys-51 distances that occur as N-cTnC molecules transition between the conformational substates that form the conformation under discussion. A significantly broadened HWHM may thus indicate that observed N-cTnC molecules are in equilibrium between the closed and open conformations, which have significantly different extents of ensemble-averaged opening. As will be demonstrated in the following sections, a combined analysis of *r* and HWHM along these lines expanded upon previous insights into the effects of strong-binding cross-bridges on N-cTnC opening and provided three major findings on the effects of SL, each validating our hypothesis.

ADP stimulated more ensemble-averaged opening in Ca^{2+}-bound N-cTnC than ATP at long sarcomere length

We will first focus on analyzing results from in situ tr-FRET experiments conducted at long, 2.2 μm SL (Fig. 1) because the results are directly comparable with observations from our prior in situ ss-FRET study (37). Changes in *r* were observed that were consistent with our prior ss-FRET observations, while changes in HWHM represented new information pertinent to changes in the protein dynamics of N-cTnC. We will now explore the changes in *r* that were observed before analyzing changes in HWHM. Fig. 1 *B* and Table 2 show that in the absence of cTnC site-II Ca^{2+} occupancy and presence of ATP, the N-cTnC ensemble exhibited a low *r* value. Introduction of Ca^{2+} resulted in a significant 7.44 ± 0.38 Å increase in *r* (Fig. 1, *B* and *C*; Table 2). This suggested that in the absence of Ca^{2+}, the N-cTnC molecules were predominantly in the closed conformation (53). Ca^{2+}-binding to N-cTnC and consequent strong actomyosin interactions then led to a considerable fraction of the N-cTnC ensemble transitioning to the open conformation of N-cTnC (4).

Subsequent treatment with Vi at pCa 4.3 to block strong cross-bridge attachment then significantly decreased *r* by 3.14 ± 0.40 Å (Fig. 1, *B* and *C*; Table 2). This strongly suggested that when strong actomyosin interactions became blocked in the presence of Ca^{2+}, the N-cTnC ensemble ended up adopting a balanced mixture of N-cTnC molecules in the closed conformation with molecules in open conformation. Such a mixture suggests that the N-cTnC ensemble is in a conformational equilibrium between the closed (53) and open (4) conformations of N-cTnC, and that changes in *r* represent shifts in equilibrium position.

Experiments with ADP provided further evidence of an N-cTnC conformational equilibrium, and indicated that strong actomyosin interactions are required to maximally stabilize the in situ N-cTnC ensemble in the open conformation. Treatment with ADP at pCa 9 (with ATP having been removed) to produce strong-binding, noncycling cross-bridges stimulated a significant increase in *r* by

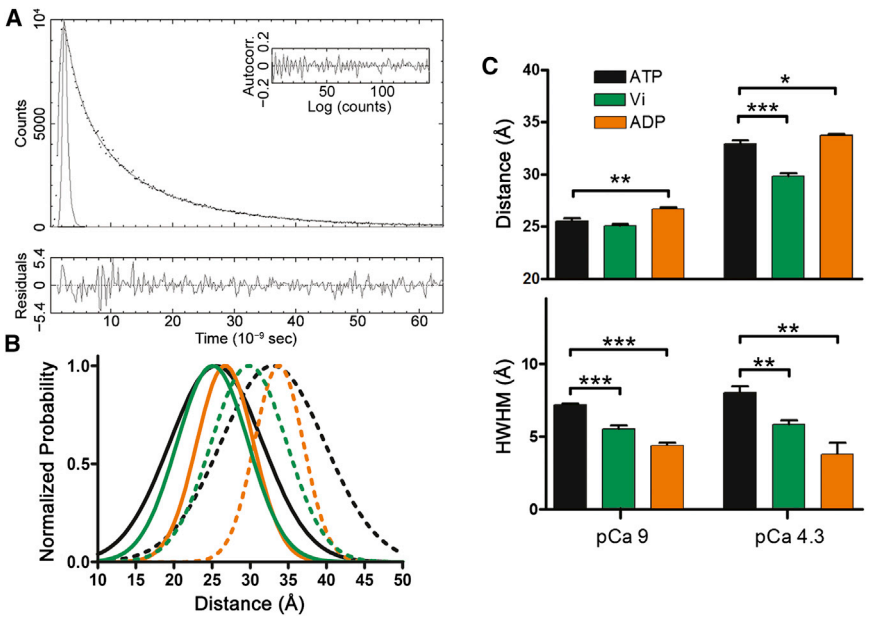

FIGURE 1 Comparison of N-cTnC Cys-13–Cys-51 distance distributions as a function of cTnC site-II Ca^{2+} occupancy and cross-bridge binding state when observed at long 2.2-μm SL in $cTnC(T13C/N51C)_{AEDANS\text{-}DDPM}$-reconstituted myocardial fibers. (*A*) (*Upper panel*) Representative trace (*black dots*) of the in situ total fluorescence intensity decay of FRET donor AEDANS in the presence of nonfluorescent acceptor DDPM, which was measured at 2.2-μm SL in the presence of Ca^{2+} (pCa 4.3) under normal cross-bridge cycling. The decay profile was fit with Eq. 1 (*gray line*). (*Inset* and *lower panel*) Autocorrelation function and residuals associated with the fitting, respectively, which were used to judge goodness of fit. (*B*) Normalized distance distributions obtained using global-curve analysis of intensity decay profiles observed under the following conditions: pCa 9 + ATP (*black solid line*), pCa 4.3 + ATP (*black dotted line*), pCa 9 + ADP (*orange solid line*), pCa 4.3 + ADP (*orange dotted line*), pCa 9 + Vi (*green solid line*), and pCa 4.3 + Vi (*green dotted line*). (Area normalized versions of these distance distributions are shown in Fig. S4 in the Supporting Material.) (*C*) As a function of whether Ca^{2+} is bound to N-cTnC, this panel shows the statistical significance of changes in *r* and HWHM that occurred because of changes in pCa level or cross-bridge binding state. Parameter values are reported as the mean ± SE. *$p < 0.05$; **$p < 0.005$; ***$p < 0.001$.

1.19 ± 0.33 Å. This was accompanied by Ca^{2+}-independent active force generation that was 1.35 ± 0.10-fold higher than what was observed for the pCa 4.3 + ATP + 2.2 μm SL test condition (Table 3). These results indicated that even in the absence of Ca^{2+}, maximal strong actomyosin interaction had led to a fraction of the N-cTnC ensemble transitioning from the closed to the open conformation. While this finding was consistent with our prior FRET work (31,37), an important fresh observation was that at pCa 4.3 and long SL and compared to cycling cross-bridges, noncycling strong-binding cross-bridges significantly further increased r by 0.81 ± 0.26 Å (Fig. 1, *B* and *C*; Table 2). Thus, even at saturating Ca^{2+} levels, the presence of weak-binding cross-bridge states during cross-bridge cycling results in a small fraction of N-cTnC molecules in the thick- and thin-filament overlap zone occupying the closed conformation. Taken together, these results with ATP, Vi, and ADP treatment at long SL strongly suggest that thin-filament regulation involves a N-cTnC conformational equilibrium that is not only highly sensitive to Ca^{2+}, but also to positive feedback from strong-binding cross-bridges.

Cycling cross-bridges caused increased N-cTnC conformational dynamics at long sarcomere length

In the form of HWHM values, tr-FRET provided information on N-cTnC protein dynamics that is inaccessible to ss-FRET. Thus, if an N-cTnC conformational equilibrium is present during thin-filament regulation and is highly sensitive to strong actomyosin interactions, HWHM values should reflect these facts. Interestingly, at long SL, the pCa-averaged HWHM value associated with cycling cross-bridges; noncycling, strong-binding cross-bridges; and noncycling, weak-binding cross-bridges was 7.62 ± 0.19, 4.09 ± 0.37, and 5.69 ± 0.16 Å, respectively, and these values were all significantly different from each other ($p < 0.01$). Thus, in the presence of cycling cross-bridges and regardless of cTnC site-II Ca^{2+} occupancy, our single Gaussian model suggested that the relative number of N-cTnC conformational substates was on average 1.86 ± 0.17-fold ($p < 0.001$) and 1.33 ± 0.05-fold ($p < 0.001$) greater than in the presence of noncycling strong and noncycling weak cross-bridges, respectively. However, no significant difference in HWHM value was noted for changes in cTnC site-II Ca^{2+} occupancy with respect to the same cross-bridge state.

TABLE 3 Force values (mean ± SE, $n = 5–6$) from cTnC(T13C/N51C)$_{AEDANS-DDPM}$-reconstituted fibers observed at pCa 9 and 4.3 as a function of XB state and SL

		Force (mN mm^{-2})	
Cross-bridge state	pCa	1.8 μm SL	2.2 μm SL
5 mM ATP	9.0	0.449 ± 0.377	8.62 ± 0.45
	4.3	20.0 ± 1.1	34.3 ± 1.6
1 mM Vi[a]	9.0	1.03 ± 0.24	8.41 ± 0.26
	4.3	1.51 ± 0.88	8.98 ± 2.01
5 mM ADP[b]	9.0	24.0 ± 2.2	43.5 ± 2.1
	4.3	22.1 ± 3.7	40.7 ± 2.2
0.5 mM Vi[a]	9.0	—	8.63 ± 1.05
	4.3	—	13.0 ± 1.9
2.5 mM ADP[b]	9.0	—	26.2 ± 2.4
	4.3	—	33.6 ± 1.2

[a]Vi solutions also contained 5 mM ATP.
[b]ATP was absent in ADP solutions.

These results indicated that the number of conformational substates being sampled by the N-cTnC ensemble was sensitive to cross-bridge state, but not cTnC site-II Ca^{2+} occupancy. Compared to Vi test conditions, ATP test conditions led to an increase in the number of N-cTnC conformational substates, whereas ADP test conditions tended to decrease them. As explored further in the Discussion below, this strongly suggests that the N-cTnC conformational equilibrium point is sensitive to the regulatory state of tropomyosin, which is itself highly sensitive to changes in strong actomyosin interaction. Cycling cross-bridges should accordingly produce the greatest variety of occupation of tropomyosin regulatory states, resulting in the highest HWHM values. In contrast, noncycling, strong-binding cross-bridges should maximally bias tropomyosin toward the open state of thin-filament regulation, leading to the lowest HWHM values.

To further evaluate the cross-bridge-state dependence of N-cTnC conformational dynamics, Cys-13–Cys-51 distance distributions were measured under varying concentrations of ADP and Vi (Fig. 2; Table 2). Martyn et al. (54) has suggested that the equilibrium of weak- and strong-binding cross-bridges during normal force generation can be altered by a change in [Vi], and changes in ADP concentration should similarly affect the stability of strong-binding states. Observed force values verified these expectations (Table 3), and the effects of the concomitant changes in strong actomyosin interaction were as follows: at both pCa 9.0 and 4.3, as Mg^{2+}-ADP was increased from 0 to 2.5 and then 5 mM to increasingly bias cross-bridges toward the strong-binding state (Fig. 2 *A*), r was increasingly raised ($p < 0.05$) and HWHM was increasingly lowered ($p < 0.05$). We inferred that while tropomyosin was being increasingly stabilized in the open state of thin-filament regulation by strong actomyosin interactions, the N-cTnC ensemble was being increasingly stabilized in the open conformation.

Furthermore, at pCa 4.3, as the concentration of Vi was increased from 0 to 0.5 and then 1 mM to increasingly disrupt strong cross-bridge attachment (Fig. 2 *B*), r was increasingly lowered ($p < 0.05$) and HWHM was increasingly lowered ($p < 0.001$). Accordingly, we inferred that while tropomyosin was being increasingly destabilized in the open state of thin-filament regulation, the N-cTnC ensemble was being increasingly transitioned toward the closed conformation of N-cTnC. Interestingly, at pCa 9, HWHM was increasingly lowered ($p < 0.01$), but no significant change in r was observed. This suggested that while cycling cross-bridges lead to increased sampling of the

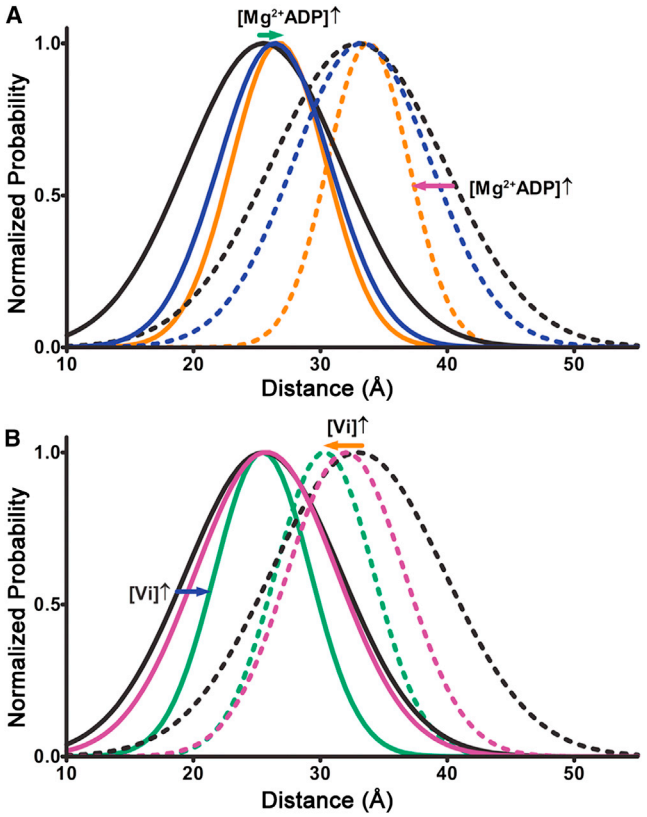

FIGURE 2 Cys-13–Cys-51 distance distributions calculated from intensity decays observed in cTnC(T13C/N51C)$_{AEDANS}$- and cTnC(T13C/N51C)$_{AEDANS\text{-}DDPM}$-reconstituted fibers set to 2.2 μm SL and exposed to intermediate and saturating concentrations of ADP and Vi. Similar to Fig. 1, the distance distributions were normalized against their peaks (area-normalized versions are shown in Fig. S5), and *solid lines* and *dashed lines* indicate measurements taken at pCa 9 and pCa 4.3, respectively. (*A*) Structural effects of 2.5 mM Mg^{2+}-ADP (*blue lines*) versus 5 mM Mg^{2+}-ADP (*orange lines*). For the purpose of visual comparison, distance distributions measured in presence of 5 mM ATP (*black lines*) are also plotted. (*Green* and *purple arrows*) How distance distributions change in response to increasing [Mg^{2+}-ADP]. (*B*) Similarly to panel *A*, the structural effects of 0.5 mM Vi (*purple lines*) versus 1.0 mM Vi (0.5 mM, *green lines*) are shown. (*Blue* and *orange arrows*) How distance distributions change in response to increasing [Vi].

open state by the N-cTnC ensemble even at pCa 9, such sampling is not stable enough to cause a change in *r* that could be picked up by the single Gaussian model. Overall, the observed changes in HWHM further indicated that in situ N-cTnC is in a conformational equilibrium in which not only cTnC site-II Ca^{2+} occupancy but also strong actomyosin interactions are required to maximally stabilize N-cTnC in the open conformation.

Reduction of sarcomere length diminished the influence of strong-binding cross-bridges on N-cTnC conformational behavior

We next tested the effect of SL on the cross-bridge-state-dependent N-cTnC conformational behavior. Interestingly, the stabilizing effects of cycling cross-bridges on N-cTnC opening noted above for 2.2 μm SL test conditions (Fig. 1 *B*, *black lines*) were attenuated at short, 1.8 μm SL (Fig. 3 *A*, *black lines*). In the presence of ATP, both *r* and HWHM became significantly decreased at pCa 4.3 when the SL was changed from 2.2 to 1.8 μm (Fig. 3 *D*). Moreover, the normalized maximal active force generated by cycling cross-bridges was reduced by 23.9 $\pm$ 6.1% when SL was reduced from 2.2 to 1.8 μm (Table 3). Thus, when strong actomyosin interaction was decreased by SL reduction, the N-cTnC conformational equilibrium was concurrently shifted away from the open conformation toward the closed conformation, which resulted in reduced ensemble-averaged opening and fewer underlying conformational substates. This observation was the first major finding that validated our hypothesis. It was interpreted to indicate that a decrease in SL decreases the orientation and ordering of cross-bridges optimal for strong actomyosin interaction (48), which leads to a reduction in 1), steady-state force development and 2), N-cTnC opening through diminished NcTnC-cTnI-Sr interaction (37).

Based on this interpretation, we next predicted that a reduction in SL should also reduce the ability of noncycling, strong-binding cross-bridges to stabilize N-cTnC opening. Further testing demonstrated that at short SL, the replacement of ATP with ADP in pCa solutions had no significant effect on either *r* or HWHM (Fig. 3 *B*); hence, SL reduction from 2.2 to 1.8 μm caused the stabilizing effects of noncycling, strong-binding cross-bridges on N-cTnC opening to become significantly diminished (Fig. 3, *C* and *D*). Therefore, this observation also validated our hypothesis and further suggested that at short SL, the effects of positive feedback regulation on N-cTnC structure are significantly diminished. The consequent destabilization of the N-cTnC ensemble in the open conformation of N-cTnC provides a fresh structural insight into why reductions in Ca^{2+} sensitivity occur alongside decreases in active force generation as SL is decreased.

Treatment with vanadate eliminated sarcomere-length-dependent structural changes in N-cTnC

If SL-dependent modulation of positive feedback regulation is critically involved in effecting length-dependent Ca^{2+} sensitivity, then chemical prevention of strong cross-bridge attachment should eliminate SL-dependent changes in N-cTnC opening altogether (55). This prediction was verified by experiments wherein Vi was used to chemically inhibit the attachment of strong cycling cross-bridges to actin (Figs. 1 and 3). As expected, at pCa 4.3 and under Vi treatment, there was no statistical difference between the *r* and HWHM values obtained at 1.8 and 2.2 μm SL (Fig. 3, *C* and *D*). Moreover, the addition of 1 mM Vi to pCa 4.3 solutions reduced *r* and HWHM at both 1.8 and 2.2 μm SLs (Figs. 3 *B* and 1 *C*); however, the Vi-induced

reduction in *r* observed at long SL was significantly greater than that observed at short SL. Therefore, the observed Vi-induced elimination of SL-modulation of N-cTnC opening represented additional evidence that implicated SL-dependent modulation of positive feedback regulation as mechanistically involved in length-dependent activation.

DISCUSSION

The orientation and ordering of myosin heads relative to their binding sites on actin are key parameters for determining the probability that cross-bridges will form strong actomyosin interactions, and biophysical evidence has been accumulating that these parameters depend on SL (48,56–58). Results from our recent in situ ss-FRET study indicated that strong actomyosin interactions lead to a stabilization of ensemble-averaged N-cTnC opening (37), from which it was inferred that strong actomyosin interactions affect the associations of tropomyosin and cTnI with actin in a manner that indirectly leads to a stabilization of the Ca^{2+}-sensitizing N-cTnC–cTnI-Sr interaction (10,24,37,59). Accordingly, we hypothesized in this study that SL-dependent modulation of strong actomyosin interactions leads to a concomitant modulation of the stabilizing effect of strong actomyosin interactions on N-cTnC opening.

Because our ss-FRET technique depends on the measurement of fluorescence intensity, it is technically challenging to test our hypothesis using this method because the fluorescence baseline is subject to change whenever the fiber being observed is stretched or slackened. To overcome this technical obstacle, we successfully modified our Güth MRS to perform in situ tr-FRET measurements, which take advantage of the fact that fluorescence lifetime is independent of fluorophore concentration. As demonstrated by our results, tr-FRET enabled us to characterize changes in the conformational behavior of N-cTnC caused by changes in cTnC site-II Ca^{2+} occupancy, cross-bridge binding state, or SL. We were also able to probe N-cTnC conformational

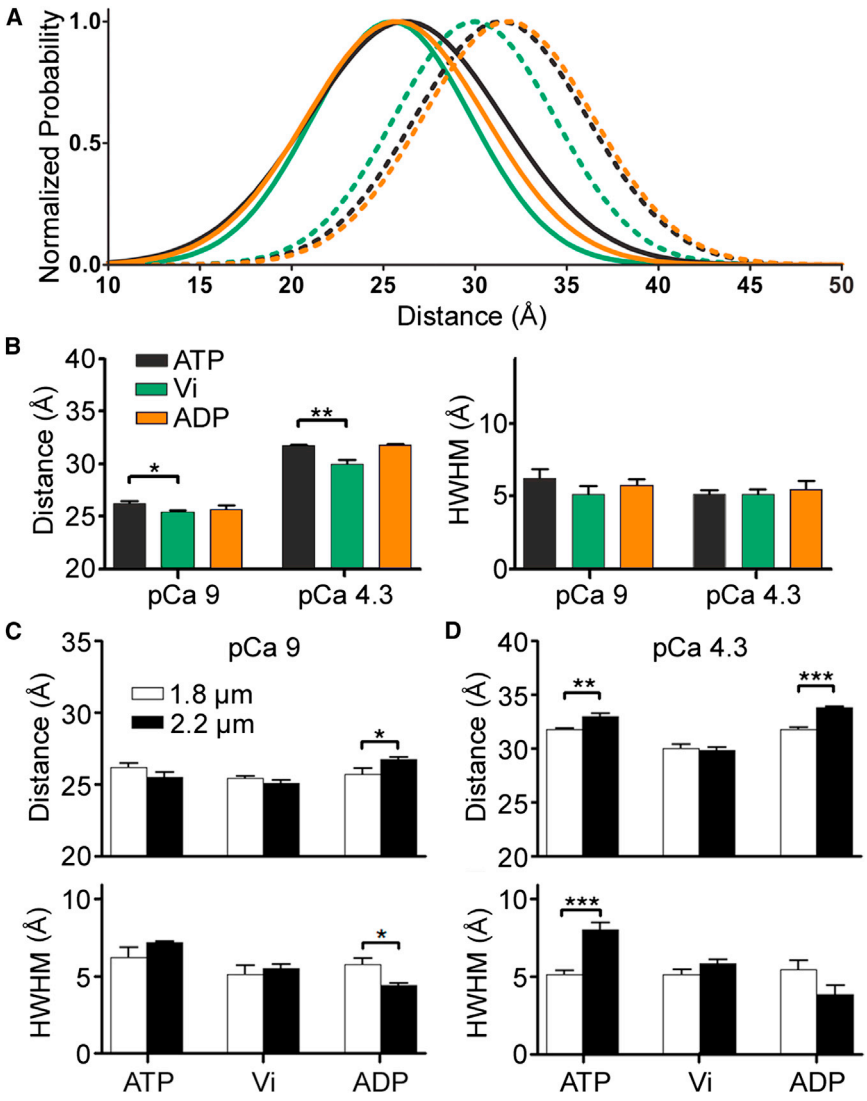

FIGURE 3 Comparison of N-cTnC Cys-13–Cys-51 distance distributions as a function of cTnC site-II Ca^{2+}-occupancy and cross-bridge state when observed at short 1.8-μm SL in cTnC(T13C/N51C)$_{AEDANS\text{-}DDPM}$-reconstituted myocardial fibers. (*A*) Normalized distance distributions obtained using global-curve analysis of intensity decay profiles observed under the following conditions: pCa 9 + ATP (*black solid line*), pCa 4.3 + ATP (*black dotted line*), pCa 9 + ADP (*orange solid line*), pCa 4.3 + ADP (*orange dotted line*), pCa 9 + Vi (*green solid line*), and pCa 4.3 + Vi (*green dotted line*). (Area-normalized versions of these distance distributions are shown in Fig. S6.) (*B*) As a function of whether Ca^{2+} is bound to N-cTnC and at 1.8 μm SL, this panel shows the statistical significance of differences in *r* and HWHM values that occurred because of changes in cross-bridge binding state. (*C* and *D*) Significance of differences in *r* and HWHM due to reduction of SL. The number of determinations was 5–6 for each group. $*p < 0.05$; $**p < 0.005$; $***p < 0.001$.

dynamics because nanosecond timescale domain structural dynamics were embedded in the high-quality, time-resolved data. The implications of our major findings on our understanding of cardiac thin-filament regulation are discussed below. Note that the conformational changes discussed are considered as ensemble averages; we make no attempt to distinguish differences between cross-bridge overlapping and nonoverlapping regions of the thin filament.

N-cTnC is in a conformational equilibrium that is shifted toward the open conformation by positive feedback regulation

In our prior ss-FRET study (37), it was posited that the stabilizing effect of positive feedback from strong-binding cross-bridges on N-cTnC opening involves an N-cTnC conformational equilibrium shift (6,9,30,37). Supporting this argument, in situ FRET distance distributions obtained here at 2.2 μm SL under ATP conditions were dramatically broader than distributions observed under ADP or Vi test conditions (Fig. 1 and Table 2). Values of r obtained under various conditions also indicated that the conformational occupancy of the N-cTnC ensemble was mixed between the closed and open conformations. These results strongly suggested that the in situ N-cTnC ensemble is in equilibrium between the closed and open conformations of N-cTnC. Moreover, the equilibrium point, as represented by both r and HWHM, was observed to be highly sensitive not just to changes in cTnC site-II Ca^{2+} occupancy, but also cross-bridge state. Hence, Ca^{2+}-binding to N-cTnC and positive feedback from strong actomyosin interactions together determine the fraction of the N-cTnC ensemble that occupies the open versus closed conformation at steady state (Fig. 4).

Because ensemble-averaged in situ N-cTnC opening is an excellent indicator of in situ thin-filament activation (37), the sensitivity of the N-cTnC conformational equilibrium to cross-bridge state strongly supports the importance of positive feedback regulation in cardiac thin-filament regulation. Our results indicated that Ca^{2+} alone was unable to fully activate the cardiac thin filament, just as argued previously by Wu et al. (60). In fact, based on ensemble-averaged N-cTnC opening at long SL, our results suggested that in the absence of strong actomyosin interactions and their effects on tropomyosin, cTnI, and cTnC structure, the thin filament is at most 52.3 $\pm$ 3.6% activated under Ca^{2+} saturation (Table 2 and see Table S1: 2.2 μm SL, pCa 4.3 + Vi vs. pCa 4.3 + ADP; calculation ignores role of overlap between thick and thin filaments). Furthermore, our previous ss-FRET Ca^{2+} titration results indicated that the Ca^{2+} sensitivity of the thin filament is depressed by $\Delta pCa_{50} = -0.26 \pm 0.05$ (mean $\pm$ standard deviation, $n = 5$) when positive feedback regulation is maximally inhibited by Vi (37). Therefore, without positive feedback regulation, the thin filament would achieve neither the level of activation in response to Ca^{2+} binding nor the Ca^{2+} sensitivity required for generating the correct amount of active force in response to normal systolic Ca^{2+} transients.

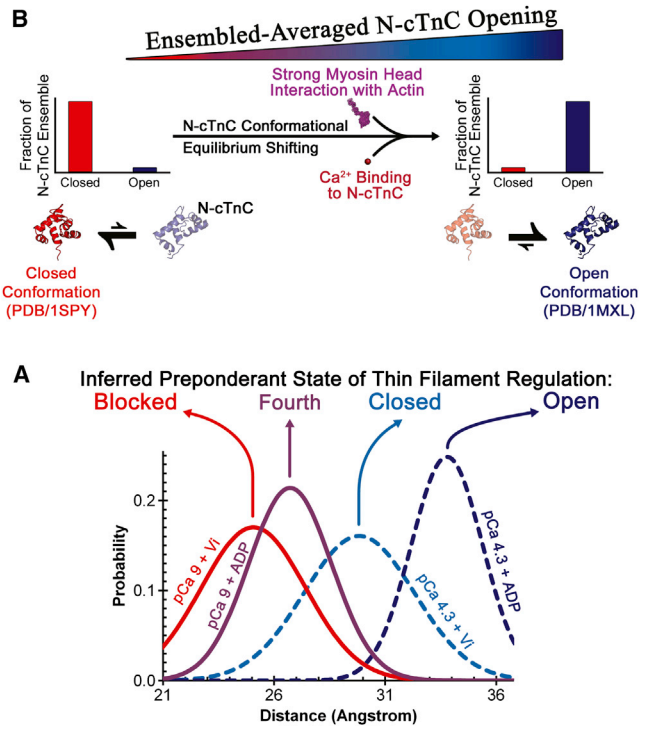

FIGURE 4 A schematic presenting our model for how changes in N-cTnC Ca^{2+} site-II occupancy and cross-bridge state lead to changes in ensemble-averaged N-cTnC opening at 2.2 μm SL. (*A*) Shown here are selected area-normalized distance distributions, which each represent a different a preponderant state of the four states of thin-filament regulation (27), as based on cTnC site-II Ca^{2+} occupancy and cross-bridge binding state. Hence, in terms of the preponderant state of thin-filament regulation, the extent of ensemble-averaged N-cTnC opening is ranked in the following order: Blocked < Fourth < Closed < Open. (*B*) We interpret the observed changes in ensemble-averaged N-cTnC opening as caused by shifts in an N-cTnC conformational equilibrium that is at work during thin-filament regulation. As explained further in the main text, Ca^{2+} binding to N-cTnC and strong cross-bridge binding to actin can each independently and allosterically lead to a shift in this equilibrium from the closed conformation of N-cTnC toward the open conformation. However, Ca^{2+} binding to N-cTnC and strong actomyosin interactions work in concert during physiological thin-filament regulation, and both are required to maximally activate the thin-filament and concomitantly shift the N-cTnC equilibrium toward the open conformation. The structures of N-cTnC presented in panel *B* were from PDB:1SPY (53) and PDB:1MXL (4), as indicated.

Myofilament length-dependent activation involves the length-dependent modulation of positive feedback regulation

Length-dependent activation is thought to be the basis of the Frank-Starling law of the heart. However, the identity of the complete mechanism underlying the SL-dependence of myocardial force production has proven complex and controversial (43,44). Contemporary hypotheses have

variously posited that SL-dependent modulation of the probability of weak cross-bridge attachments (61,62), probability of strong cross-bridge attachments (55,63), extent to which myosin head orientation and ordering are favorable for the formation of strong actomyosin interactions (48), thin-filament-intrinsic cooperativity (62,64), structural changes in thin-filament proteins (65), titin strain (66), or thin-filament compliance (67–69) are important determinants in length-dependent activation. It is likely that all of these proposed mechanisms may contribute to length-dependent activation, but new insights are needed to clarify the cause-and-effect relationships that link these processes into a unified molecular mechanism. The biophysical data presented in this study help to address this need by contributing new insights into the effects of changes in SL and cross-bridge state on the conformational behavior of N-cTnC. We observed that increased SL leads to increased ensemble-averaged N-cTnC opening only when strong-binding cross-bridges are present. Because shifting of the N-cTnC ensemble toward the open conformation is known to lead to increased Ca^{2+} sensitivity (37–42), these observations represent a fresh structural insight into why increased SL leads to increased thin-filament Ca^{2+} sensitivity.

Our results provide additional support to the argument that length-dependent activation involves the modulation of strong cross-bridge binding and concomitant positive feedback regulation by changes in SL (24,45). This argument was recently advanced by small-angle x-ray diffraction measurements by Farman et al. (48) on the conformational behavior of cross-bridges in intact right ventricular trabeculae from rat. Their findings indicated that SL is positively correlated with an optimal average orientation and ordering of myosin heads for strong cross-bridge attachment to the thin filament. Consistent with this, we observed that decreased SL led to reduced strong actomyosin interaction, as implied by decreased force, concomitant with decreased ensemble-averaged N-cTnC opening. We interpret this N-cTnC structural effect as due to reduced positive feedback regulation.

In our model of positive feedback regulation (37), we infer that strong actomyosin interactions are allosterically transduced into stabilization of N-cTnC opening through changes in the associations of tropomyosin and cTnI with actin. Tropomyosin is shifted toward the open state and interactions between cTnI and actin/tropomyosin become disrupted. This is further inferred to indirectly promote increased interaction between cTnI-Sr and N-cTnC, which shifts the N-cTnC conformational equilibrium toward the open conformation of N-cTnC.

Finally, these structural changes are inferred to allosterically spread along the thin filament through tropomyosin-mediated couplings between regulatory units. In keeping with this model, because strong actomyosin interactions are influenced by SL, it is inferred that the allosteric structural changes they stimulate in tropomyosin, cTnI, and N-cTnC are consequently also influenced by SL. Thus, the proposed SL-dependent positive feedback regulation mechanism could explain why cTnI isoform, thin-filament cooperativity, and strong cross-bridge binding have all been implicated as determinants in the length-dependent activation mechanism. Titin may be inferred as important for determining how changes in SL modulate strong actomyosin interaction, and thin-filament compliance might be expected to modulate the protein-protein interactions involved in positive feedback regulation. Hence, complete characterization of the unified mechanism for length-dependent activation now not only seems possible, but inevitable.

Growing evidence that absence of strong cross-bridge binding results in the loss of the sarcomere-length-dependence of thin-filament Ca^{2+} sensitivity

Our Vi-associated results presented in this study contribute more-explicit structural evidence that Vi-mediated inhibition of strong-binding cross-bridge attachment to actin attenuates the effects of SL on thin-filament Ca^{2+} sensitivity. Smith et al. (55) previously used in situ linear dichroism to show that increasing levels of Vi resulted in decreasing extents of cross-bridge-dependent N-cTnC structural changes and decreasing dependencies of the Ca^{2+} sensitivity of contractile force on SL. Their results corroborated earlier linear dichroism measurements by Martyn and Gordon (26) showing that a saturating level of Vi eliminated SL-dependent changes in cTnC structure and the SL-dependence of Ca^{2+} sensitivity. Our observation here that 1 mM Vi treatment causes a loss of SL-induced changes in N-cTnC opening strongly indicates that the cTnC structural changes being observed by Smith et al. (55) and Martyn and Gordon (26) were associated with changes in N-cTnC opening and corresponding cross-bridge-dependent stabilization of the Ca^{2+}-sensitizing N-cTnC–cTnI-Sr interaction (37).

Inhibitors of strong cross-bridge attachment other than Vi also appear to exert attenuating effects on the length dependence of Ca^{2+} sensitivity. Kurihara et al. (70) used aequorin-injected right ventricular papillary muscle from ferret to show that 10 mM BDM eliminated SL-dependent changes in Ca^{2+} binding to N-cTnC, and consistent with findings obtained using Vi, this effect of BDM treatment also leads to the conclusion that length-dependent activation involves positive feedback from the attachment of strong-binding cross-bridges. Farman et al. (62) reported that increasing concentrations of blebbistatin of up to 1 μM had a slightly steeper effect on the relationship between EC_{50} and maximal force at 2.0 μm SL than at 2.2 μm SL. However, the authors further found that this difference in steepness was statistically insignificant with $p = 0.2$, as determined by Student's t-test. These findings suggest that an important

experiment would be to directly compare the effects of Vi, BDM, and blebbistatin on the SL-dependence of N-cTnC opening. Unfortunately, such a direct comparison was not possible in this study, because the ultraviolet light required to excite AEDANS would rapidly inactivate blebbistatin (71). As of this writing, we are developing a FRET scheme relying on a longer-wavelength donor fluorophore that will make such a comparison possible in the future.

CONCLUSIONS

Our biophysical data presented here implicates positive feedback regulation as modulated by changes in SL, making it therefore mechanistically involved in myofilament length-dependent activation. In light of growing biophysical evidence that cooperativity is intrinsic to the thin filament such that strong actomyosin interactions may not be needed to achieve a steep relation between force and Ca^{2+} level (37,47,55), the uniquely high degree that cardiac thin-filament activation depends on strong cross-bridge binding (60) may therefore instead be an impressive evolutionary adaptation that helps facilitate length-dependent activation.

We note that much remains to be determined about the cause-and-effect relationships that link changes in SL, to changes in strong actomyosin interaction, to changes in N-cTnC opening. We expect that the posttranslational state of thin and thick filaments, titin strain, thin-filament cooperativity, thin-filament compliance, and protein isoform specific effects all play an important mechanistic role in these relationships. This is because all of these properties influence the allosteric interplay among cycling cross-bridges and tropomyosin, cTnI, and cTnC. Therefore, the reason why the mechanism underlying myofilament length-dependent activation has proven so difficult to establish is that many factors are working together in giving rise to the emergent property that is cardiac myofilament length-dependent activation.

SUPPORTING MATERIAL

Supporting Materials and Methods, six equations, six figures, and one table are available at http://www.biophysj.org/biophysj/supplemental/S0006-3495(14)00628-6.

We thank the laboratory of Jaak Panksepp for generously providing the rats that were used in this study. We are also grateful to Sheri Six for her assistance with animal handling.

This work was supported, in whole or in part, by National Institutes of Health grants No. R01 HL80186-5S1 (to W.-J.D.), No. R01 HL64035 (to R.J.S.), and No. R21 HL109693 (to W.-J.D.), and also by the M. J. Murdock Charitable Trust (to W.-J.D.). The study described in this manuscript was also supported by award No. T32GM008336 from the U.S. National Institute of General Medical Sciences.

The content is solely the responsibility of the authors and does not necessarily represent the official views of the National Institute of General Medical Sciences or the National Institutes of Health.

SUPPORTING CITATIONS

Refs. (72–76) appear in the Supporting Material.

REFERENCES

1. Tobacman, L. S. 1996. Thin filament-mediated regulation of cardiac contraction. *Annu. Rev. Physiol.* 58:447–481.
2. Gordon, A. M., E. Homsher, and M. Regnier. 2000. Regulation of contraction in striated muscle. *Physiol. Rev.* 80:853–924.
3. Wei, B., and J. P. Jin. 2011. Troponin T isoforms and posttranscriptional modifications: Evolution, regulation and function. *Arch. Biochem. Biophys.* 505:144–154.
4. Li, M. X., L. Spyracopoulos, and B. D. Sykes. 1999. Binding of cardiac troponin-I147-163 induces a structural opening in human cardiac troponin-C. *Biochemistry.* 38:8289–8298.
5. Dong, W. J., J. Xing, …, H. C. Cheung. 1999. Conformation of the regulatory domain of cardiac muscle troponin C in its complex with cardiac troponin I. *J. Biol. Chem.* 274:31382–31390.
6. Behrmann, E., M. Müller, …, S. Raunser. 2012. Structure of the rigor actin-tropomyosin-myosin complex. *Cell.* 150:327–338.
7. Kobayashi, T., M. Kobayashi, …, J. H. Collins. 2000. Inhibitory region of troponin I: Ca^{2+}-dependent structural and environmental changes in the troponin-tropomyosin complex and in reconstituted thin filaments. *Biochemistry.* 39:86–91.
8. Dong, W. J., J. M. Robinson, …, H. C. Cheung. 2003. Ca^{2+}-induced conformational transition in the inhibitory and regulatory regions of cardiac troponin I. *J. Biol. Chem.* 278:8686–8692.
9. Robinson, J. M., W. J. Dong, …, H. C. Cheung. 2004. Switching of troponin I: Ca^{2+} and myosin-induced activation of heart muscle. *J. Mol. Biol.* 340:295–305.
10. Xing, J., M. Chinnaraj, …, W. J. Dong. 2008. Structural studies of interactions between cardiac troponin I and actin in regulated thin filament using Förster resonance energy transfer. *Biochemistry.* 47:13383–13393.
11. Xing, J., J. J. Jayasundar, …, W. J. Dong. 2009. Förster resonance energy transfer structural kinetic studies of cardiac thin filament deactivation. *J. Biol. Chem.* 284:16432–16441.
12. Zhou, Z., K.-L. Li, …, W.-J. Dong. 2012. Structural dynamics of C-domain of cardiac troponin I protein in reconstituted thin filament. *J. Biol. Chem.* 287:7661–7674.
13. Hoffman, R. M., T. M. Blumenschein, and B. D. Sykes. 2006. An interplay between protein disorder and structure confers the Ca^{2+} regulation of striated muscle. *J. Mol. Biol.* 361:625–633.
14. Potter, J. D., Z. Sheng, …, J. Zhao. 1995. A direct regulatory role for troponin T and a dual role for troponin C in the Ca^{2+} regulation of muscle contraction. *J. Biol. Chem.* 270:2557–2562.
15. Huxley, H. E. 1972. Structural changes in the actin-and myosin-containing filaments during contraction. *Cold Spring Harb. Symp. Quant. Biol.* 37:361–376.
16. Haselgrove, J. C. 1972. X-ray evidence for a conformational change in the actin-containing filaments of vertebrate striated muscle. *Cold Spring Harb. Symp. Quant. Biol.* 37:341–352.
17. Holmes, K. C. 1995. The actomyosin interaction and its control by tropomyosin. *Biophys. J.* 68:2S–7S.
18. Lehman, W., R. Craig, and P. Vibert. 1994. Ca^{2+}-induced tropomyosin movement in Limulus thin filaments revealed by three-dimensional reconstruction. *Nature.* 368:65–67.
19. Lehman, W., V. Hatch, …, R. Craig. 2000. Tropomyosin and actin isoforms modulate the localization of tropomyosin strands on actin filaments. *J. Mol. Biol.* 302:593–606.
20. Poole, K. J. V., G. Evans, …, K. C. Holmes. 1995. The effect of cross-bridges on the calcium sensitivity of the structural change of the regulated thin filament. *Biophys. J.* 68:A365.

21. Gordon, A. M., and E. B. Ridgway. 1987. Extra calcium on shortening in barnacle muscle. Is the decrease in calcium binding related to decreased cross-bridge attachment, force, or length? *J. Gen. Physiol.* 90:321–340.

22. Güth, K., and J. D. Potter. 1987. Effect of rigor and cycling cross-bridges on the structure of troponin C and on the Ca^{2+} affinity of the Ca^{2+}-specific regulatory sites in skinned rabbit psoas fibers. *J. Biol. Chem.* 262:13627–13635.

23. Hannon, J. D., D. A. Martyn, and A. M. Gordon. 1992. Effects of cycling and rigor crossbridges on the conformation of cardiac troponin C. *Circ. Res.* 71:984–991.

24. Moss, R. L., M. Razumova, and D. P. Fitzsimons. 2004. Myosin cross-bridge activation of cardiac thin filaments: implications for myocardial function in health and disease. *Circ. Res.* 94:1290–1300.

25. Miki, M., H. Hai, …, T. Wakabayashi. 2004. Fluorescence resonance energy transfer between points on actin and the C-terminal region of tropomyosin in skeletal muscle thin filaments. *J. Biochem.* 136:39–47.

26. Martyn, D. A., and A. M. Gordon. 2001. Influence of length on force and activation-dependent changes in troponin c structure in skinned cardiac and fast skeletal muscle. *Biophys. J.* 80:2798–2808.

27. Lehrer, S. S. 2011. The 3-state model of muscle regulation revisited: is a fourth state involved? *J. Muscle Res. Cell Motil.* 32:203–208.

28. Dong, W. J., J. Xing, …, H. C. Cheung. 2001. Ca^{2+} induces an extended conformation of the inhibitory region of troponin I in cardiac muscle troponin. *J. Mol. Biol.* 314:51–61.

29. Dong, W. J., J. M. Robinson, …, H. C. Cheung. 2003. Kinetics of conformational transitions in cardiac troponin induced by Ca^{2+} dissociation determined by Förster resonance energy transfer. *J. Biol. Chem.* 278:42394–42402.

30. Robinson, J. M., H. C. Cheung, and W. Dong. 2008. The cardiac Ca^{2+}-sensitive regulatory switch, a system in dynamic equilibrium. *Biophys. J.* 95:4772–4789.

31. Dong, W. J., J. J. Jayasundar, …, H. C. Cheung. 2007. Effects of PKA phosphorylation of cardiac troponin I and strong crossbridge on conformational transitions of the N-domain of cardiac troponin C in regulated thin filaments. *Biochemistry.* 46:9752–9761.

32. Bacchiocchi, C., and S. S. Lehrer. 2002. Ca^{2+}-induced movement of tropomyosin in skeletal muscle thin filaments observed by multi-site FRET. *Biophys. J.* 82:1524–1536.

33. Davis, J. P., C. Norman, …, S. B. Tikunova. 2007. Effects of thin and thick filament proteins on calcium binding and exchange with cardiac troponin C. *Biophys. J.* 92:3195–3206.

34. Reference deleted in proof.

35. Wang, H., J. M. Chalovich, and G. Marriott. 2012. Structural dynamics of troponin I during Ca^{2+}-activation of cardiac thin filaments: a multi-site Förster resonance energy transfer study. *PLoS ONE.* 7:e50420.

36. Akhter, S., Z. Zhang, and J.-P. Jin. 2012. The heart-specific NH2-terminal extension regulates the molecular conformation and function of cardiac troponin I. *Am. J. Physiol. Heart C.* 302:H923–H933.

37. Rieck, D. C., K.-L. Li, …, W.-J. Dong. 2013. Structural basis for the in situ Ca^{2+} sensitization of cardiac troponin C by positive feedback from force-generating myosin cross-bridges. *Arch. Biochem. Biophys.* 537:198–209.

38. Gollapudi, S. K., R. Mamidi, …, M. Chandra. 2012. The N-terminal extension of cardiac troponin T stabilizes the blocked state of cardiac thin filament. *Biophys. J.* 103:940–948.

39. Holroyde, M. J., S. P. Robertson, …, J. D. Potter. 1980. The calcium and magnesium binding sites on cardiac troponin and their role in the regulation of myofibrillar adenosine triphosphatase. *J. Biol. Chem.* 255:11688–11693.

40. Robertson, I. M., Y. B. Sun, …, B. D. Sykes. 2010. A structural and functional perspective into the mechanism of Ca^{2+}-sensitizers that target the cardiac troponin complex. *J. Mol. Cell. Cardiol.* 49:1031–1041.

41. Jayasundar, J. J., J. Xing, …, W. J. Dong. 2014. Molecular dynamics simulations of the cardiac troponin complex performed with FRET distances as restraints. *PLoS ONE.* 9:e87135.

42. Wang, D., I. M. Robertson, …, M. Regnier. 2012. Structural and functional consequences of the cardiac troponin C L48Q Ca^{2+}-sensitizing mutation. *Biochemistry.* 51:4473–4487.

43. de Tombe, P. P., R. D. Mateja, …, T. C. Irving. 2010. Myofilament length dependent activation. *J. Mol. Cell. Cardiol.* 48:851–858.

44. Cordina, N. M., C. K. Liew, …, L. J. Brown. 2013. Effects of calcium binding and the hypertrophic cardiomyopathy A8V mutation on the dynamic equilibrium between closed and open conformations of the regulatory N-domain of isolated cardiac troponin C. *Biochemistry.* 52:1950–1962.

45. Gillis, T. E., D. A. Martyn, …, M. Regnier. 2007. Investigation of thin filament near-neighbor regulatory unit interactions during force development in skinned cardiac and skeletal muscle. *J. Physiol.* 580: 561–576.

46. Lakatta, E. G. 1987. Starling's law of the heart is explained by an intimate interaction of muscle length and myofilament calcium activation. *J. Am. Coll. Cardiol.* 10:1157–1164.

47. Shitaka, Y., C. Kimura, and M. Miki. 2005. The rates of switching movement of troponin T between three states of skeletal muscle thin filaments determined by fluorescence resonance energy transfer. *J. Biol. Chem.* 280:2613–2619.

48. Farman, G. P., D. Gore, …, P. P. de Tombe. 2011. Myosin head orientation: a structural determinant for the Frank-Starling relationship. *Am. J. Physiol. Heart Circ. Physiol.* 300:H2155–H2160.

49. Campbell, K. S. 2011. Impact of myocyte strain on cardiac myofilament activation. *Pflugers Arch.* 462:3–14.

50. Mocz, G. 1989. Vanadate-mediated photocleavage of rabbit skeletal myosin. *Eur. J. Biochem.* 179:373–378.

51. Fukuda, N., T. Terui, …, S. Kurihara. 2009. Titin and troponin: central players in the Frank-Starling mechanism of the heart. *Curr. Cardiol. Rev.* 5:119–124.

52. Strauss, J. D., C. Zeugner, …, J. C. Rüegg. 1992. Troponin replacement in permeabilized cardiac muscle. Reversible extraction of troponin I by incubation with vanadate. *FEBS Lett.* 310:229–234.

53. Spyracopoulos, L., M. X. Li, …, B. D. Sykes. 1997. Calcium-induced structural transition in the regulatory domain of human cardiac troponin C. *Biochemistry.* 36:12138–12146.

54. Martyn, D. A., L. Smith, …, M. Regnier. 2007. The effects of force inhibition by sodium vanadate on cross-bridge binding, force redevelopment, and Ca^{2+} activation in cardiac muscle. *Biophys. J.* 92:4379–4390.

55. Smith, L., C. Tainter, …, D. A. Martyn. 2009. Cooperative cross-bridge activation of thin filaments contributes to the Frank-Starling mechanism in cardiac muscle. *Biophys. J.* 96:3692–3702.

56. McDonald, K. S., and R. L. Moss. 1995. Osmotic compression of single cardiac myocytes eliminates the reduction in Ca^{2+} sensitivity of tension at short sarcomere length. *Circ. Res.* 77:199–205.

57. Fuchs, F., and Y.-P. Wang. 1996. Sarcomere length versus interfilament spacing as determinants of cardiac myofilament Ca^{2+} sensitivity and Ca^{2+} binding. *J. Mol. Cell. Cardiol.* 28:1375–1383.

58. Farman, G. P., J. S. Walker, …, T. C. Irving. 2006. Impact of osmotic compression on sarcomere structure and myofilament calcium sensitivity of isolated rat myocardium. *Am. J. Physiol. Heart Circ. Physiol.* 291:H1847–H1855.

59. Galińska-Rakoczy, A., P. Engel, …, W. Lehman. 2008. Structural basis for the regulation of muscle contraction by troponin and tropomyosin. *J. Mol. Biol.* 379:929–935.

60. Wu, S., J. Liu, …, K. A. Taylor. 2010. Electron tomography of cryofixed, isometrically contracting insect flight muscle reveals novel actin-myosin interactions. *PLoS ONE.* http://dx.doi.org/10.1371/journal.pone.0012643.

61. Cremo, C. R., G. T. Long, and J. C. Grammer. 1990. Photocleavage of myosin subfragment 1 by vanadate. *Biochemistry.* 29:7982–7990.

62. Farman, G. P., E. J. Allen, …, P. P. de Tombe. 2010. The role of thin filament cooperativity in cardiac length-dependent calcium activation. *Biophys. J.* 99:2978–2986.

63. Fukuda, N., H. Kajiwara, …, S. Kurihara. 2000. Effects of MgADP on length dependence of tension generation in skinned rat cardiac muscle. *Circ. Res.* 86:E1–E6.

64. Grammer, J. C., C. R. Cremo, and R. G. Yount. 1988. UV-induced vanadate-dependent modification and cleavage of skeletal myosin subfragment 1 heavy chain. 1. Evidence for active site modification. *Biochemistry.* 27:8408–8415.

65. Tachampa, K., H. Wang, …, P. P. de Tombe. 2007. Cardiac troponin I threonine 144: role in myofilament length dependent activation. *Circ. Res.* 101:1081–1083.

66. Martyn, D. A., B. B. Adhikari, …, L. C. Yu. 2004. Response of equatorial x-ray reflections and stiffness to altered sarcomere length and myofilament lattice spacing in relaxed skinned cardiac muscle. *Biophys. J.* 86:1002–1011.

67. Huxley, H. E., A. Stewart, …, T. Irving. 1994. X-ray diffraction measurements of the extensibility of actin and myosin filaments in contracting muscle. *Biophys. J.* 67:2411–2421.

68. Wakabayashi, K., Y. Sugimoto, …, Y. Amemiya. 1994. X-ray diffraction evidence for the extensibility of actin and myosin filaments during muscle contraction. *Biophys. J.* 67:2422–2435.

69. Campbell, K. S. 2009. Interactions between connected half-sarcomeres produce emergent mechanical behavior in a mathematical model of muscle. *PLOS Comput. Biol.* 5:e1000560.

70. Kurihara, S., Y. Saeki, …, N. Sudo. 1990. Effects of length change on intracellular Ca^{2+} transients in ferret ventricular muscle treated with 2,3-butanedione monoxime (BDM). *Jpn. J. Physiol.* 40:915–920.

71. Sun, Y. B., F. Lou, and M. Irving. 2009. Calcium- and myosin-dependent changes in troponin structure during activation of heart muscle. *J. Physiol.* 587:155–163.

72. Fabiato, A., and F. Fabiato. 1979. Calculator programs for computing the composition of the solutions containing multiple metals and ligands used for experiments in skinned muscle cells. *J. Physiol. (Paris).* 75:463–505.

73. Chandra, M., M. L. Tschirgi, …, K. B. Campbell. 2007. Interaction between myosin heavy chain and troponin isoforms modulate cardiac myofiber contractile dynamics. *Am. J. Physiol. Regul. Integr. Comp. Physiol.* 293:R1595–R1607.

74. Ford, S. J., R. Mamidi, …, M. Chandra. 2012. Effects of R92 mutations in mouse cardiac troponin T are influenced by changes in myosin heavy chain isoform. *J. Mol. Cell. Cardiol.* 53:542–551.

75. Liao, R., C. K. Wang, and H. C. Cheung. 1992. Time-resolved tryptophan emission study of cardiac troponin I. *Biophys. J.* 63:986–995.

76. Dale, R. E., J. Eisinger, and W. E. Blumberg. 1979. The orientational freedom of molecular probes. The orientation factor in intramolecular energy transfer. *Biophys. J.* 26:161–193.

SUPPORTING MATERIAL

In Situ Time-Resolved FRET Reveals Effects of Sarcomere Length on Cardiac Thin-Filament Activation

King-Lun Li[a], Daniel Rieck[a], R. John Solaro[c], Wenji Dong[a, b]

[a]Gene and Linda Voiland School of Chemical Engineering and Bioengineering, Washington State University, Pullman, WA 99164, USA

[b]Integrative Neuroscience and Physiology, Washington State University, Pullman, WA 99164, USA

[c]The Department of Physiology and Biophysics, Center for Cardiovascular Research, College of Medicine, University of Illinois at Chicago, Chicago, IL 60612, USA.

SUPPORTING MATERIALS AND METHODS

Preparation of Proteins

The recombinant double cysteine mutant cTnC(T13C/N51C) from a rat cDNA clone was subcloned into a pET-3d vector, which was then transformed into BL21(DE3) cells (Invitrogen) and expressed under isopropyl β-D-1-thiogalactopyranoside induction. The expressed protein was purified and fluorescently labeled with the FRET donor AEDANS using thiol-reactive 5-(iodoacetamidoethyl)aminonaphthelene-1-sulfonic acid as previously described (1). Unlabeled, singly, and doubly labeled cTnC(T13C/N51C) were separated using a DEAE column. The concentrated singly labeled fraction, $cTnC(T13C/N51C)_{AEDANS}$ (donor-only sample), was collected and divided into two aliquots. One aliquot was subsequently labeled with a large excess of the FRET acceptor DDPM at the other cysteine to obtain the doubly labeled $cTnC(T13C/N51C)_{AEDANS\text{-}DDPM}$ (donor-acceptor sample), and the other aliquot was saved as a reference sample (donor-only sample). The labeling ratio of the donor-only sample was verified to be >95% using UV–vis spectroscopy and the $\varepsilon_{325\ nm}$ of AEDANS, which is 6000 $cm^{-1}\ M^{-1}$.

Animal Handling Protocols

The handling of all the experimental animals followed the institutional guidelines and protocols approved by the Animal Care and Use Committee and the Office of Laboratory Animal Welfare, National Institutes of Health. Our muscle fiber study also followed the established guidelines of and was approved by the Washington State University Institutional Animal Care and Use Committee.

Preparation of pCa Solutions

The reagent concentrations for the pCa (−log of free Ca^{2+} concentration) solutions were calculated based on the program by Fabiato (2). Highly relaxing solution contained the following: 50 BES, 30.83 K-Propionate, 10 NaN_3, 20 EGTA, 6.29 $MgCl_2$, 6.09 Na_2ATP. Maximally activating solution (pCa 4.3) contained the following (in mM): 50 BES, 5 NaN_3, 10 EGTA, 10.11 $CaCl_2$, 6.61 $MgCl_2$, 5.95 Na_2ATP and 51 K-propionate. Relaxing solution (pCa 9.0) had a similar composition (in mM): 50 BES, 5 NaN_3, 10 EGTA, 0.024 $CaCl_2$, 6.87 $MgCl_2$, 5.83 Na_2ATP and 71.14 K-propionate. For crossbridge inhibiting solution, 1 mM sodium Vi was added to the above pCa solutions. For ADP-mediated non-cycling, strong-binding cross-bridge solutions, ATP was removed from relaxing and maximally activating solutions, and 5 mM Mg^{2+}-ADP was added in its place. The ionic strength of all pCa solutions was 180 mM. In addition, protease inhibitors including 5 μM bestatin, 2 μM E-64, 10 μM leupeptin, and 1 μM pepstatin were also added to the pCa solutions (3).

Preparation of Detergent-Skinned Cardiac Muscle Fibers

Left ventricular papillary bundles from adult (6–8 months in age) Long–Evans rats were prepared using protocol established by Chandra and coworkers (4). Animals were deeply anesthetized by inhalation of isoflurane and hearts were quickly excised and placed into ice-cold highly relaxing solution that contained the following: 50 mM N,N-bis (2-hydroxyethyl)-2-aminoethane-sulfonic acid (BES), pH 7.0, 30.83 mM K propionate, 10 mM Na azide, 20 mM ethylene glycol tetraacetic acid (EGTA), 6.29 mM $MgCl_2$, 6.09 mM Na_2ATP, 1.0 mM DTT, and 20 mM 2,3-butanedione monoxime. A fresh protease inhibitors including 4 μM benzamidine-HCl, 5 μM bestatin, 2 μM E-64, 10 μM leupeptin, 1 μM pepstatin and 200 μM phenylmethylsulfonyl fluoride were added to the solution. Papillary muscle bundles were carefully removed from the left ventricles of rat hearts. Muscle fibers (~150–200 μm in diameter and 2.0 mm in length) were dissected and skinned overnight at 4 °C using 1% triton X-100 in highly relaxing solution.

Reconstitution of detergent-skinned, cTnC-extracted rat myocardial fibers with modified cTnC

Incorporation of modified cTnC into cardiac muscle fibers was based on a extraction/reconstitution method described previously (1). Endogenous cTnC in detergent-skinned rat cardiac muscle fibers was first removed by incubating fibers in an extraction solution for 2.5-3 hours. The extraction solution contained (in mM): 5 trans-1,2-cyclohexanediamine-N,N,N',N'-tetraacetic acid (CDTA), 40 Tris-HCl (pH 8.4.), 0.6 NaN_3, 0.005 bestatin, 0.002 E-64, 0.01 leupeptin, and 0.001 pepstatin. cTnC-extracted fibers were washed with the relaxing solution and then incubated overnight in cTnC solution (1.5 mg mL^{-1}) containing either donor-only or donor-acceptor modified cTnC(T13C/N51C) in the presence of myosin light chain-2 (0.76 mg mL^{-1}). Ca^{2+}-

activated maximal tension was measured in pCa 4.3 solution for cTnC-depleted fibers to determine the residual tension and for exogenous cTnC reconstituted fibers to determine recovery of maximum tension.

SDS–PAGE and Western blotting analysis of reconstitution levels of modified cTnC in cardiac muscle

Based on previously described methods (1), detergent-skinned cardiac muscle fibers reconstituted with modified cTnC were incubated in 10 μL of a protein extraction buffer per 1 muscle fiber on ice for 1 hr. Skinned fibers that had not undergone extraction were similarly incubated to create a negative control. The protein extraction buffer contained 2.5% SDS, 10% glycerol, 50 mM Tris base (pH 6.8 at 4 °C), 1 mM DTT, 1 mM phenylmethylsulfonyl fluoride, 4 mM benzamidine HCl, 5 μM bestatin, 2 μM E-64, 10 μM leupeptin, and 1 μM pepstatin. After incubation, samples were sonicated for 20 min in a water bath at 4 °C and centrifuged at 10k rpm. The supernatants were loaded to SDS–PAGE gels for Western blotting analysis. Sample loading amounts were standardized between each sample by estimating total protein concentration and further optimized based on relative actin concentrations. Equal amounts of protein were loaded and separated on a 4–20% SDS–PAGE gel. Separated proteins were then transferred to polyvinylidene difluoride membrane. The membrane was incubated in a blocking solution containing Tris-buffered saline with 2% tween-20 (TBS/T) and 5% dry milk. The blocked membrane was then treated with 1:5000 dilution of primary mouse anti-rat antibody against cTnC (Fitzgerald 10-T78A) in blocking solution overnight. Excess primary antibody was successively rinsed away by washing the membrane several times with TBS/T. The primary antibody treated membrane was further treated with 1:5000 dilution of horseradish peroxidase conjugated sheep anti-mouse antibody (Amersham NTF825) in blocking solution for 1 hour. An enhanced luminol-based chemiluminescent (ECL) kits (Amersham ECL Western Blotting Analysis System RPN 2108) was then used to detect the level of cTnC in the fiber samples.

Experimental Apparatus

A previously described Güth muscle research system (1) was used in this study to simultaneously make biomechanical and optical measurements. Isometric force measurements were conducted using a force transducer (SI Heidelberg KG7A) capable of measuring 5 mN with a resonance frequency of 500 Hz. Detergent-skinned left ventricular cardiac muscle fiber samples from normal adult male Long–Evans rats were mounted between the force transducer and a stationary tweezer. A quartz perfusion cuvette with a diameter of 1 mm was slipped over the preparation and pCa solution was continuously perfused through the mounted fiber during experimentation. The SL of the fiber was adjusted to either 1.8 or 2.2 μm using He-Ne laser diffraction measurements. The temperature of the pCa solution within the cuvette was held a 20 ± 0.2 °C using a bipolar temperature controller (Cell MicroControls TC2BIP) coupled with a cooling/heating module (Cell MicroControls CH). To perform time-resolved fluorescence measurements with chemically skinned muscle fibers containing modified cTnC, the MRS was modified by replacing the photomultiplier tube in its PH1A microscope photometer with a TBX picosecond photon detection module (HORIBA Jobin Yvon). To eliminate uncontrolled factors that can affect the conformational state of N-cTnC during rising phase of force development, time-resolved fluorescence measurements were made when fiber force reached steady-state (Fig. 1B). Excitation light at 340 nm was projected onto the muscle fiber through the cuvette from a NanoLED (HORIBA Jobin Yvon N-340) with a <1.2 ns pulse width. The total fluorescence emission from the central area of the muscle fiber was isolated for measurement using the PH1A microscope window slit and optics to focus the light onto the TBX, and fluorescence intensity decays of muscle fibers containing either donor-only or donor-acceptor modified cTnC(T13C/N51C) were processed and recorded by a FluoroHub-B (HORIBA Jobin Yvon). With this instrument setup, a total of 10,000 photon counts at peak channel for each decay collection was achieved in 1–1.5 min.

Simultaneous Measurement of Isometric Force and Time-Resolved Fluorescence Intensity in Detergent-Skinned Cardiac Muscle Fibers

To eliminate experimental uncertainty from variations in handling between fiber preparations, isometric force and time-resolved fluorescence measurements were observed at both 1.8 and 2.2 μm SLs with the same muscle fiber according to the following measurement protocol. SL was adjusted to either 1.8 or 2.2 μm SL using laser diffraction and subjected to an initial cycle of activation and relaxation, after which the SL was readjusted if necessary. Half of our measurements were started at 1.8 μm SL, whereas the other half was started at 2.2 μm SL. Isometric force and a fluorescence intensity decay were then synchronously, digitally recorded as the fiber was subjected to pCa 4.3 solution at the chosen SL. After completion of the measurement, highly relaxing solution, containing 20 mM EGTA, was used to completely relax the fiber, and then force and an intensity decay were recorded. The SL of the fiber was then adjusted to the opposite SL of the one that was initially chosen; for example, if the measurement had started with 1.8 μm SL, then the fiber was adjusted to a SL of 2.2 μm. Recordings were then made with pCa 4.3 and pCa 9.0 solutions in the same fashion as before. The order with which SLs were tested was

later found to exert no discernable effect on the outcome of experiments. This same measurement protocol was used to perform tr-FRET measurements of N-cTnC opening in the presence of cycling cross-bridges (5 mM Mg-ATP); Mg^{2+}-ADP-induced non-cycling, strong-binding cross-bridges (5 mM Mg-ADP + 0 mM ATP); and vanadate-induced non-cycling, weak-binding cross-bridges (1 mM Vi + 5 mM Mg-ATP).

There are some important experimental design considerations for using Vi to inhibit strong cross-bridge binding, which are as follows. Myosin can be UV photocleaved by the tetrameric form of aqueous Vi (5-7), but photocleavage kinetics are greatly attenuated by the presence of ATP and actin (8) such that photocleavage is not a concern on the timescales involved in our experiments here. This was confirmed here by the fact that following the tr-FRET measurement protocol, maximal force could be recovered on average to 88.0 ± 2.3% regardless of test condition. Furthermore, when higher Vi concentrations are used (~10 mM), polymeric species of vanadate becomes significantly present in solution, and it is this polymeric species of vanadate that has been implicated as extracting cTnI and cTnC from the troponin complex (9). Because of our lower concentration of Vi at 1 mM, no extraction of cTnI and cTnC was expected. Confirming this, no significant change in passive tension at pCa 9 was observed following the tr-FRET measurement protocol conducted in the presence of Vi, indicating that no appreciable Vi-mediated extraction of cTnI and cTnC had occurred.

Determination of Inter-Probe Distance Distrubutions from Measured Fluorescence Intensity Decays

The AEDANS-DDPM inter-probe distance distribution associated with a specific test condition was determined as follows. The AEDANS excited-state decays observed for the donor-only samples were fitted with a multi-exponential function (10):

$$I_D(t) = \sum_{i=1}^{n} \alpha_i \, e^{-t\,\tau_i^{-1}} \tag{S1}$$

where the α_i represents the fractional amplitude associated with each correlation time τ_i contributing that contributes to the overall excited-state decay process. In the presence of the non-fluorescent acceptor DDPM, the AEDANS excited-state decays observed for donor−acceptor samples were fit to the following equation using GlobalCurve analysis software (11):

$$I_{DA}(t) = \frac{\int_0^{\infty} P(r)\left(\sum_{i=1}^{n} \alpha_{D_i} \, e^{-\frac{t}{\tau_{D_i}}\left(1+\left(\frac{R_0}{r}\right)^6\right)}\right) dr}{\int_0^{\infty} P(r)\, dr} \tag{S2}$$

where r is the distance between the donor and acceptor fluorophores; α_{Di} and τ_{Di} are the fractional amplitude and correlation time parameters, respectively, determined for AEDANS in the absence of DDPM; and R_o is the Förster critical distance at which energy transfer is 50% efficient. $P(r)$ is the probability distribution of inter-probe distances, and in this study we assume it to be a single Gaussian as follows:

$$P(r) = \frac{1}{Z\,\sigma\sqrt{2\pi}} e^{-\frac{1}{2}\left(\frac{r-\bar{r}}{\sigma}\right)^2} \tag{S3}$$

where r is the mean distance and σ is the standard deviation of the distribution. $P(r)$ is normalized by area, and Z is the normalization factor. The half width at half maximum (*HWHM*) of the distribution is given by $HWHM = 1.1772\sigma$. In practice, the integration limits in Eq. 3 are not from 0 to ∞, and the integral is instead calculated over a range of distances from r_{min} to r_{max} with the lower limit being about 5 Å.

The Förster distance R_o in Eq. 2 was calculated from the spectral properties of AEDANS and DDPM:

$$R_0 = (8.79\times10^{-5}) n^{-4} Q \kappa^2 J \tag{S4}$$

where n is the refractive index of the solution and was taken as 1.4, Q is the donor quantum yield, κ^2 is the orientation factor, and J is the spectral overlap integral that is given by

$$J = \frac{\int F_D(\lambda)\,\varepsilon_A(\lambda)\,\lambda^4\, d\lambda}{\int F_D(\lambda)\, d\lambda} \tag{S5}$$

where $F_D(\lambda)$ is the fluorescence intensity of the donor at wavelength λ and $\varepsilon_A(\lambda)$ is the molar absorptivity of the acceptor at λ. J was calculated by numerical integration. Dynamic averaging and the associated value of ⅔ for κ^2 were assumed, which is valid when donor and acceptor probes tumble rapidly and randomly over the course of the measurement, which is a condition that we expected since the Cys-13 and Cys-51 of cTnC are located in surface-exposed loops. To ensure that the average orientations of the probes attached to Cys-13 and Cys-51 did not change significantly between different test conditions, which would result in unknown changes in κ^2 between conditions, the potential for a change in κ^2 was assessed by measuring the anisotropy of AEDANS under each test condition (12) (see below). The contribution of potential differences in κ^2 to changes in FRET efficiency between different states was found to be minimal (Fig. S1).

Measurement of *In Situ* Fluorescence Anisotropy

Time-resolved fluorescence anisotropy measurements were performed on chemically skinned, cTnC-extracted muscle fibers reconstituted with $cTnC(T13C/N51C)_{AEDANS}$. Because DDPM is non-fluorescent, its orientation within the muscle fiber could not be assessed using anisotropy measurements. However, our labeling scheme results in a random attachment of AEDANS to either Cys-13 or Cys-51 in $cTnC(T13C/N51C)_{AEDENS}$, so it is

likely that AEDENS anisotropies observed in donor-only samples are a good representative of probe orientation within $cTnC(T13C/N51C)_{AEDENS/DDPM}$. To measure AEDANS time-resolved anisotropy decays, the MRS was first modified by placing a pair of optical polarizers within the excitation and emission light paths. To collect time-resolved fluorescence anisotropy decays, upon excitation with vertically polarized 340 nm light oriented along axis of the fiber, vertically and horizontally polarized emissions of 480 nm from the reconstituted muscle fibers were recorded separately by manually changing orientation of the emission polarizer every 4 min with a total of 16 min of data collection. Each set of total fluorescence intensity decays was combined to generate a time-resolved anisotropy decay using anisotropy analysis software provide by HORIBA Jobin Yvon. The same software was used to fit the anisotropy decays to the following equation (10,13):

$$r_{anis} = r_0 \sum_{i=1}^{n} \alpha_i \, e^{-t \Phi_i^{-1}} \qquad \text{(S6)}$$

where r_0 is the limiting anisotropy and α_i is the fractional amplitude of each correlation time (Φ_i) that contributes to the overall anisotropy decay. Results are shown in Fig. S2.

SUPPORTING REFERENCES

1. Rieck, D. C., K.-L. Li, Y. Ouyang, R. J. Solaro, and W.-J. Dong. 2013. Structural basis for the in situ Ca^{2+} sensitization of cardiac troponin C by positive feedback from force-generating myosin cross-bridges. *Arch. Biochem. Biophys.* 537:198-209.
2. Fabiato, A., and F. Fabiato. 1979. Calculator programs for computing the composition of the solutions containing multiple metals and ligands used for experiments in skinned muscle cells. *J. Physiol. (Paris)* 75:463-505.
3. Chandra, M., M. L. Tschirgi, S. J. Ford, B. K. Slinker, and K. B. Campbell. 2007. Interaction between myosin heavy chain and troponin isoforms modulate cardiac myofiber contractile dynamics. *Am. J. Physiol.* 293:R1595-1607.
4. Ford, S. J., R. Mamidi, J. Jimenez, J. C. Tardiff, and M. Chandra. 2012. Effects of R92 mutations in mouse cardiac troponin T are influenced by changes in myosin heavy chain isoform. *J. Mol. Cell. Cardiol.* 53:542-551.
5. Grammer, J. C., C. R. Cremo, and R. G. Yount. 1988. UV-induced vanadate-dependent modification and cleavage of skeletal myosin subfragment 1 heavy chain. 1. Evidence for active site modification. *Biochemistry* 27:8408-8415.
6. Mocz, G. 1989. Vanadate-mediated photocleavage of rabbit skeletal myosin. *Eur. J. Biochem.* 179:373-378.
7. Cremo, C. R., G. T. Long, and J. C. Grammer. 1990. Photocleavage of myosin subfragment 1 by vanadate. *Biochemistry* 29:7982-7990.
8. Muhlrad, A., Y. M. Peyser, and I. Ringel. 1991. Effect of actin, ATP, phosphates, and pH on vanadate-induced photocleavage of myosin subfragment 1. *Biochemistry* 30:958-965.
9. Strauss, J. D., C. Zeugner, J. E. Van Eyk, C. Bletz, M. Troschka, and J. C. Rüegg. 1992. Troponin replacement in permeabilized cardiac muscle reversible extraction of troponin I by incubation with vanadate. *FEBS Lett.* 310:229-234.
10. Liao, R., C. K. Wang, and H. C. Cheung. 1992. Time-resolved tryptophan emission study of cardiac troponin I. *Biophys. J.* 63:986-995.
11. Dong, W.-J., J. R. Robinson, E. C.-Y. Lin, B. Ruzsics, J. Xing, and H. C. Cheung. 2004. Ca^{2+}-induced opening of the N-domain of cTnC in regulated cardiac thin filament. *Biophys. J.* 86:396a.
12. Dale, R. E., J. Eisinger, and W. E. Blumberg. 1979. The orientational freedom of molecular probes. The orientation factor in intramolecular energy transfer. *Biophys. J.* 26:161-193.
13. Zhou, Z., K.-L. Li, D. Rieck, Y. Ouyang, M. Chandra, and W.-J. Dong. 2012. Structural dynamics of C-domain of cardiac troponin I protein in reconstituted thin filament. *J. Biol. Chem.* 287:7661-7674.

Table S1: Cys-13–Cys-51 distance distributions observed in cTnC(N13C/T51C)$_{AEDANS-DDPM}$-reconstituted fibers under different biochemical conditions. Normalized parameter values are shown and given as mean ± SEM.

Cross-bridge state	pCa	Normalized *r* [a]		Normalized *HWHM* [b]	
		1.8 μm SL	2.2 μm SL	1.8 μm SL	2.2 μm SL
5 mM ATP	9.0	0.09 ± 0.03	0.00 ± 0.04	0.84 ± 0.09	0.97 ± 0.01
	4.3	0.79 ± 0.05	1.00 ± 0.03	0.74 ± 0.06	1.08 ± 0.05
1 mM Vi[c]	9.0	−0.01 ± 0.01	−0.06 ± 0.01	0.69 ± 0.08	0.74 ± 0.03
	4.3	0.60 ± 0.05	0.58 ± 0.04	0.69 ± 0.04	0.79 ± 0.04
5 mM ADP[d]	9.0	0.02 ± 0.05	0.16 ± 0.02	0.77 ± 0.06	0.59 ± 0.03
	4.3	0.84 ± 0.02	1.11 ± 0.01	0.74 ± 0.08	0.51 ± 0.10
0.5 mM Vi[c]	9.0	–	0.03 ± 0.02	–	0.88 ± 0.02
	4.3	–	0.87 ± 0.02	–	0.73 ± 0.06
2.5 mM ADP[d]	9.0	–	0.12 ± 0.03	–	0.70 ± 0.01
	4.3	–	1.04 ± 0.03	–	0.86 ± 0.05

[a] *r* is the mean distance associated with the distribution (see Eq. 3). Normalized values were calculated by taking the absolute *r* value observed under 5 mM ATP, pCa 9, and 2.2 μm SL as "0"; whereas "1" was taken as the absolute *r* value observed under 5 mM ATP, pCa 4.3, and 2.2 μm SL.

[b] *HWHM* denotes the half width at half maximum (see Eq. 3 and following text). Normalized *HWHM* values were determined according to the equation: $HWHM_{norm} = HWHM_{raw} / (r_{max} - r_{min})$. The value of r_{max} was taken as 32.97 from the pCa 4.3 + 5 mM ATP + 2.2 μm SL condition (see Table 1 of main text), whereas the value of r_{min} was taken as 25.53 from the pCa 9 + 5 mM ATP + 2.2 μm SL condition.

[c] Vi solutions also contained 5 mM ATP.

[d] ATP was absent in ADP solutions.

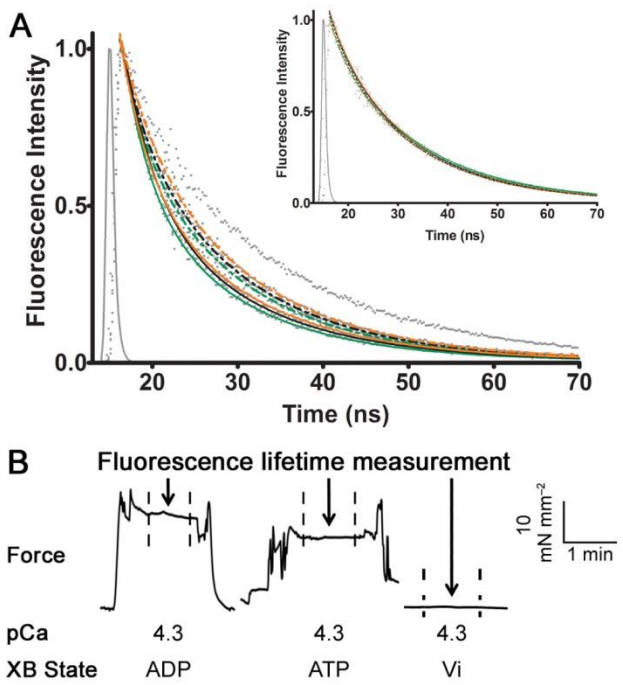

Figure S1. Representative traces of simultaneously recorded isometric force and total fluorescence intensity decay from skinned rat left ventricular papillary muscle reconstituted with either cTnC(T13C/N51C)$_{AEDANS}$ or cTnC(T13C/N51C)$_{AEDANS\text{-}DDPM}$. Measurements were taken at a SL of 2.2 µm and pCa 9 and pCa 4.3 under the biochemical conditions indicated below the force trace in panel B. (A) *Gray dots* are used to plot each raw intensity decay profile. In the main panel, *lines* represent fittings of Eqn. 1 to raw decay profiles and also indicate traces for fibers reconstituted with cTnC(T13C/N51C)$_{AEDANS\text{-}DDPM}$. *Solid lines* and *dashed lines* indicate measurements taken at pCa 9 and pCa 4.3, respectively. *Green lines*, *orange lines*, and *black lines* indicate that fibers were treated with 1 mM Vi, 5 mM ADP-Mg, or 6.13 mM ATP, respectively. The *inset* graph shows traces and fittings for cTnC(T13C/N51C)$_{AEDANS}$ fibers tested under the same conditions. (B) Arrows and dashed lines indicate how fluorescence intensity decays were measured when active force had reached steady state. Force and time magnitudes are indicated by the horizontal and vertical bars. The maximal active force developed by cTnC(T13C/N51C)$_{AEDANS\text{-}DDPM}$-reconstituted fibers was 25.6 ± 1.8 mN mm^{-2}, which was not significantly different from the 28.4 ± 3.6 mN mm^{-2} maximal active force developed by cTnC(wt)-reconstituted fibers (p = 0.1192).

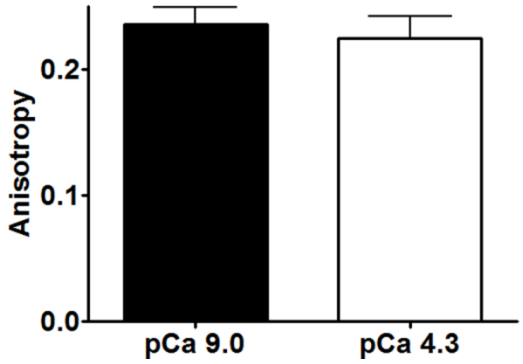

Figure S2: Anisotropy of cTnC(13C/51C)$_{AEDANS-DDPM}$ measured *in situ* under conditions of normal cross-bridge cycling.

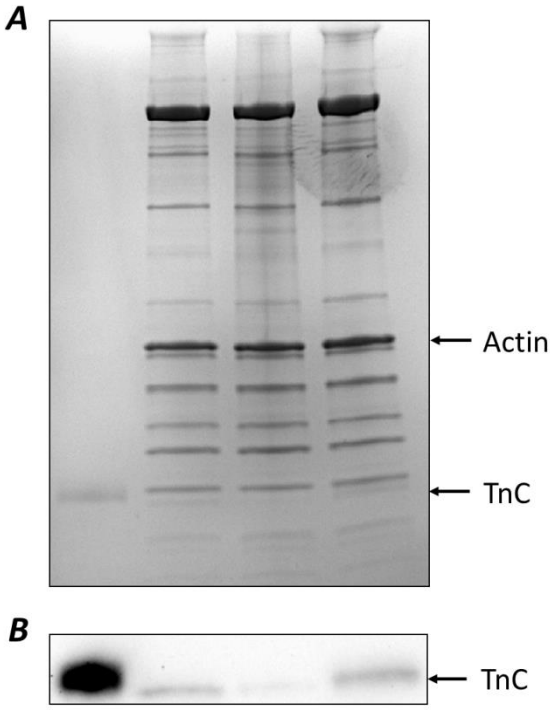

Figure S3. Assessment of cTnC incorporation in reconstituted muscle fibers. Starting from the left, *lane* 1 represents purified recombinant cTnC(wt). *Lane* 2, 3, and 4 indicate samples from skinned, CDTA treated, and cTnC(13C/N51C)$_{\text{AEDENS-DDPM}}$ reconstituted muscle fibers, respectively. (A) Coomassie blue stain was used to reveal the total protein content in the SDS-PAGE gel. (B) Anti-cTnC antibody was used to assess the extents of endogenous cTnC extraction and cTnC(13C/N51C)$_{\text{AEDENS-DDPM}}$ incorporation into reconstituted fibers. Image J software was used to analyze the protein band intensities in lane 2 to 4.

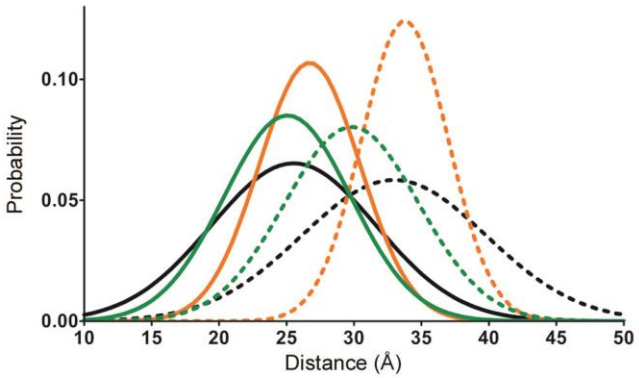

Figure S4. Area normalized versions of the N-cTnC Cys-13–Cys-51 distance distributions observed at 2.2 µm SL and shown in Fig. 1B of the main text. Conditions are as follows: pCa 9 + ATP (*black solid line*), pCa 4.3 + ATP (*black dotted line*), pCa 9 + ADP (*orange solid line*), pCa 4.3 + ADP (*orange dotted line*), pCa 9 + Vi (*green solid line*), and pCa 4.3 + Vi (*green dotted line*).

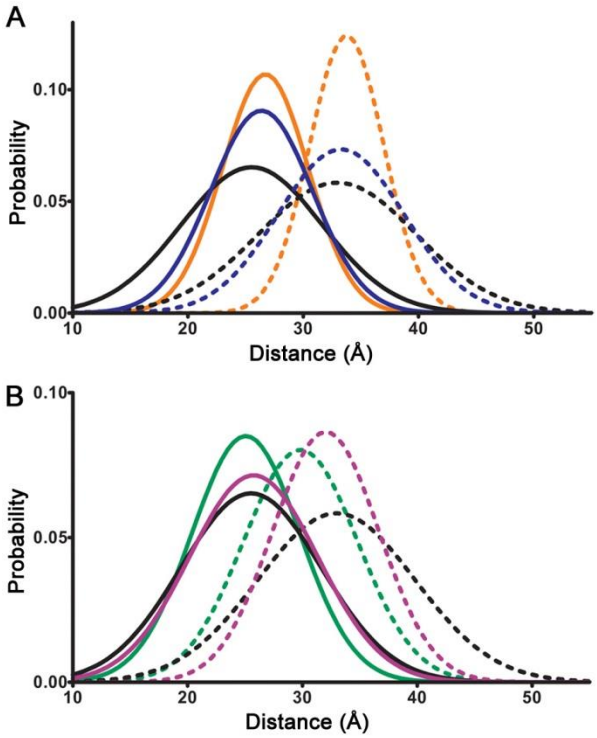

Figure S5. Area normalized versions of the N-cTnC Cys-13–Cys-51 distance distributions shown in Fig. 2 of the main text, which were observed at 2.2 µm SL under intermediate and saturating concentrations of ADP and Vi. (A) Conditions are as follows: pCa 9 + ATP (*black solid line*), pCa 4.3 + ATP (*black dotted line*), pCa 9 + 2.5 mM ADP (*blue solid line*), pCa 4.3 + 2.5 mM ADP (*blue dotted line*), pCa 9 + 5 mM ADP (*orange solid line*), and pCa 4.3 + 5 mM ADP (*orange dotted line*). (B) Conditions are: pCa 9 + ATP (*black solid line*), pCa 4.3 + ATP (*black dotted line*), pCa 9 + 0.5 mM Vi + ATP (*purple solid line*), pCa 4.3 + 0.5 mM Vi + ATP (*purple dotted line*), pCa 9 + 1 mM Vi + ATP (*green solid line*), and pCa 4.3 + 1 mM Vi + ATP (*green dotted line*).

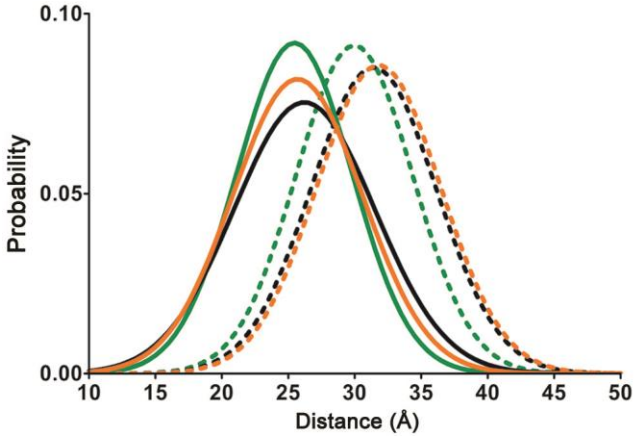

Figure S6. Area normalized versions of the N-cTnC Cys-13–Cys-51 distance distributions observed at 1.8 µm SL and shown in Fig. 5A of the main text. Conditions are as follows: pCa 9 + ATP (*black solid line*), pCa 4.3 + ATP (*black dotted line*), pCa 9 + ADP (*orange solid line*), pCa 4.3 + ADP (*orange dotted line*), pCa 9 + Vi (*green solid line*), and pCa 4.3 + Vi (*green dotted line*).